AFRL-SR-BL-TR-98-

0505

REPORT DOCUMENTATION P...

...ved
...04-0188

1. AGENCY USE ONLY (Leave blank)

2. REPORT DATE

3. REPORT TYPE AND DATES COVERED
FINAL 01 May 96 TO 30 Apr 98

4. TITLE AND SUBTITLE
MODIFICATION OF MATEPIAL SURFACE USING PLASMA-ENHANCED ION BEAMS

5. FUNDING NUMBERS
F49620-96-1-0181
D700/01
62712E

6. AUTHOR(S)
DR V. BYSTRITSKII

7. PERFORMING ORGANIZATION NAME(S) AND ADDRESS(ES)
DEPT OF PHYSICS
UNIVERSITY OF CALIFORNIA AT IRVINE
4129 PHYSICAL SCIENCES 2
IRVINE CA 92697-4575

8. PERFORMING ORGANIZATION REPORT NUMBER

9. SPONSORING MONITORING AGENCY NAME(S) AND ADDRESS(ES)
AFOSR/NL
110 Duncan Ave Room b115
Bolling AFB DC 20332-8050

Maj Hugh C. De Long

10. SPONSORING MONITORING AGENCY REPORT NUMBER

19980630 041

11. SUPPLEMENTARY NOTES

12a. DISTRIBUTION AVAILABILITY STATEMENT
Approved for public release; distribution unlimited.

12b. DISTRIBUTION CODE

13. ABSTRACT (Maximum 200 words)

Final report presents review of the experimental data obtained during the first and the second year of the 2- years research effort on Application of Microsecond Plasma Opening Switch (MPOS) Technology for Materials Surface Modification. Following second year programmatic plan, formulated in the conclusion of the 1-st year report we we focused our effort on study of aluminum alloys modification (A12024, 6061, 7075), including enhancement of their corrosion resistance, testing feasibility of treatment of non-planar surfaces, testing new technology of composite film formation (TiAl) and improvement of aluminum alloys bulk fatigue properties. The ion beam parameters used are 250 keV energy, and current and energy densities of 150 A/cm2 and 2.2 J/cm2, respectively. Characterization of the treated samples showed structural changes to a depth of about +1 micron. We demonstrated factor of 3 enhancement of corrosion resistance for the treated Al alloys samples, as measured by their mass loss. EDAX and Auger analysis of irradiated Al samples with pre-deposited thin Ti films indicate that mixing due to ion beam irradiation occurs to a depth of up to 1 micron. The systematic study on the bulk tensile and fatigue properties of the MPOS treated A12024, A17075 alloy samples were carried out both in air and in corrosive media.

14. SUBJECT TERMS

15. NUMBER OF PAGES

16. PRICE CODE

17. SECURITY CLASSIFICATION OF REPORT	18. SECURITY CLASSIFICATION OF THIS PAGE	19. SECURITY CLASSIFICATION OF ABSTRACT	20. LIMITATION OF ABSTRACT
(U)	(U)	(U)	(UL)

The measurements indicate no deterioration of the fatigue life time in the air for the MPOS treated samples, compared with non-treated. In the same time significant enhancement of fatigue life time for the treated 7075 alloy in corrosive media (1.5 times higher in fatigue limit) was registered. For the 2024 alloy the enhancement of fatigue lifetime was detectable only for higher stresses.

Final Report

Modification of Material Surfaces Using Plasma Enhanced Ion Beams

Submitted to:
To: Dr. Steven Wax
DARPA/DSO
Assistant Director, Materials Sci Dept
3701 North Fairfax Drive,
Arlington VA 22203-0001

Program manager
Hugh De Long, Mayor, USAF,
Air Force Office of Scientific Research
110 Duncan Ave, Rm B115,
Bolling AFB, DC, 20332-8050

Award Number: F49620-96-1-0181

Submitted by:

Vitaly Bystritskii,
Eusebio Garate,
Enrique Lavernia
University of California, Irvine, CA, 92697
Department of Physics & Astronomy,
Department of Engineering & Material Sciences

Irvine, CA, 92697,

June, 1998

Table of content

Figures Captions

Fig. 1. Computer simulations of surface layer temperature dynamics for ion beam interaction with Fe (a) and Al (b) samples for HPPIB energy of 180 keV and its composition of : 40% H^+, 30% C^{++}. The ion current density is: ● - 150 A/cm2; ◆ 100 A/cm^2; - 60 A/cm^2

Fig. 2 Schematic of the HPIB System

1. Primary energy source
2. Gas pressurized spark gap
3. Insulating vacuum interface
4. Cathode electrode
5. Anode electrode
6. Plasma guns
7. Ion diagnostics
8. Material samples
9. Pumping port
10. Current diagnostic
11. Power supply for plasma guns

Fig. 3 a) Sample Dimension of rectangular Sample (American Standards ASTM E8M-88): b = 6 mm, Lo = 25 mm, Lc = 32 mm, r = 6 mm, Lt = 100 mm; **b)** Arrangement for Four-Point Bending Fatigue Test. L= 45 mm, sample width b = 4 mm, thickness h =1.6 mm.

Fig. 4 Surface structure of ion beam treated carbon steel (a), j_i = 100 A/cm^2, E = 200 keV; and b) Al6061-T6 alloy , j_i = 80 A/cm^2, E_i = 200 keV.

Fig. 5 X-ray diffraction patterns from the a) treated and b) untreated surfaces of Al alloy Al2024, j_i = 80 A/cm^2, E_i = 200 keV

Fig. 6 SEM of cross-sectioned Al2024-T3. A nickel coating of 15 μm is placed on the surface to facilitate cross-sectioning. The approximately 2 μm darkened region below the nickel is the ion beam affected layer.

Fig. 7 Microhardness of carbon steel samples with different carbon content, treated with j = 80-110 A/cm^2, E = 250 KeV

Fig. 8 Effects of current density on microhardness of the treated surfaces of a) non-hardened and b) pre-hardened (lower) carbon steels.

Fig. 9 Microhardness on the cross-sections of carbon steel and stainless steel samples

Figure 10. Anodic polarization curves for 6061 (left) and 2024 aluminum (right) alloys. The ion beam energy is 250 keV.

Figure 11: Dependence of the melted and evaporated layers thickness from the ion current density.

Figure 12: SEM of 6061-T6 aluminum covered with a 500 nm thick film of titanium. The upper SEM is the untreated portion of the sample and the lower SEM is the treated portion of the sample. The ion beam energy is 250 keV and the current density is 150 A/cm^2.

Figure 13: EDAX meausurements of Ti content for the untreated Ti/Al sample (upper curve) and treated one (lower curve).

Figure 14: Auger profile of a 6061 aluminum substrate covered with a thin titanium film of 500 nm thickness after irradiation with a 250 keV, 150 A/cm2 ion beam

Figure 15. S-N curves obtained bending fatigue tests of Al2024-T3 Alclad in atmospheric air

Figure 16. S-N curves obtained from bending fatigue tests of Al7075 in 0.5 M NaCl aqueous solution: O- MPOS treated, ● - untreated samples. The upper curve is air fatigue for both types of samples.

Figure 17. S-N curves obtained from bending fatigue tests of Al2024-T3 Alclad alloy in 0.5 M NaCl aqueous solution: O - MPOS treated, ● - untreated samples.

Figure 18. Indurance limits for MPOS treated and untreated Al7075-T6 alloy in the air and aqueous salt conditions.

Abstract

Final report presents review of the experimental data obtained during the first and the second year of the 2-years research effort on Application of Microsecond Plasma Opening Switch (MPOS) Technology for Materials Surface Modification. Following second year programmatic plan, formulated in the conclusion of the 1-st year report we focused our effort on study of aluminum alloys modification (Al2024, 6061,7075), including enhancement of their corrosion resistance, testing feasibility of treatment of non-planar surfaces, testing new technology of composite film formation (TiAl) and improvement of aluminum alloys bulk fatigue properties. The ion beam parameters used are < 250 keV energy, and current and energy densities of 150 A/cm^2 and < 2.2 J/cm^2, respectively.

Characterization of the treated samples showed structural changes to a depth of about ≈1 micron. We demonstrated factor of 3 enhancement of corrosion resistance for the treated Al alloys samples, as measured by their mass loss. EDAX and Auger analysis of irradiated Al samples with pre-deposited thin Ti films indicate that mixing due to ion beam irradiation occurs to a depth of up to 1 micron. The systematic study on the bulk tensile and fatigue properties of the MPOS treated Al2024, Al7075 alloy samples were carried out both in air and in corrosive media. The measurements indicate no deterioration of the fatigue life time in the air for the MPOS treated samples, compared with non-treated. In the same time significant enhancement of fatigue life time for the treated 7075 alloy in corrosive media (1.5 times higher in fatigue limit) was registered. For the 2024 alloy the enhancement of fatigue lifetime was detectable only for higher stresses.

I. Introduction

Pulsed-power technology and High Power Pulsed Ion Beams (HPPIB) in particular look promising for material surface modification, particularly for the enhancement of their corrosion and erosion resistance. Earlier experiments using HPPIB have demonstrated improved surface properties on carbon and stainless steels, aluminum and polymers [1-11]. HPPIB irradiation can result in considerable microstructure changes of the materials, resulting in surface micro-hardening for a variety of carbon steels [1,2,6,7]. Conventional technologies for generating ion beams include pulsed power high current ion diodes (vacuum or plasma filled) [2, 3, 9], low current semi-continuous ion beams [6], and low density ($10^{10\text{-}11}$ cm^{-3}) plasma filled configurations [5]. The main objective of our 2-year research effort was to:

- demonstrate during the first year the feasibility and effectiveness of a novel pulsed ion beam irradiation approach for material modification, which uses the plasma enhanced, high power, multi-directional pulsed ion beam, produced in a Microsecond Plasma Opening Switch (MPOS) configuration. This approach for the production of the high power ion beam pulse stands out in the field and has very important and real advantages over competing technologies. To do this we fulfilled design and fabrication of the experimental system; tested and characterized the device; demonstrated enhancement of a corrosion resistance for aluminum alloys with flat geometry; fulfilled scaling studies on microhardness enhancement for several steel alloys with flat geometry.
- fulfill during the second year scaling study for MPOS treated Al alloys samples (Al 2024, 6061, and 7075) on variation of their bulk properties (tensile strength for tension and bending); fatigue life time and corrosion limited life time in various media pertinent to their pre treatment by the ion beam in the MPOS.

2. Basics of Material Treatment with HPPIB

The interaction of the HPPIB with material surfaces is a complicated process and some fundamental aspects remain to be solved, especially with regards to the practical application of high-power ion beams to engineering materials. As the ions interact with the material surface, they lose energy to the electrons and atoms of the material by collisions with the atoms in the surface layer. Most of the energy then transfers into thermal energy and heats the material surface layer. Under certain conditions blisters or craters are formed and melting is produced on the irradiated material surfaces.

Pronounced morphological alterations of surfaces may occur during ion bombardment. Typical surface structures may involve cones, depressions, ridges and trenches, facet type with their size exceeding the projectile range by orders of magnitude[12]. It should be pointed out that some of the processes that take place during the ion bombardment have already found wide applications in industrial technology.[12,13] For example, ion sputtering and ion implantation are successfully used in the manufacture of semiconductor devices and integrated circuits for microelectronics.[12] HPPIB treatment of surfaces differs qualitatively and quantitatively from conventional ion implantation technology. HPPIB treatment is a pure thermal process that does not alter the atomic composition of the sample, and is characterized with extreme power density flow (10^6-10^8 W/cm^2) and very short duration (10^{-7}-10^{-6} s). The combination of these two features results in rapid heating, melting, and partial ablation of a thin surface layer, followed by a very fast resolidification. Typical cooling rates for the process can be between 10^9 to 10^{10} K/s. In principle, these cooling rates are sufficient to cause amorphous layer formation and the production of non-equilibrium microstructures including nano-crystalline and metastable phases. It seems that these phenomena are responsible for significantly improved corrosion, wear and hardness properties of various materials.

A rough estimate of the energy density required for rapid heating to melting of a sample, based on simple physical principles, gives W >1 to 1.5 J/cm^2. This corresponds to a current density of about 50 A/cm^2 for a 100 ns pulse at 300 keV. An 300 keV proton energy would require a current density of about 90 A/cm^2 due mostly to the longer range of the protons and the thermal diffusion. Intensive evaporation (ablation) occurs when the temperature reaches a critical value, for iron it is 2700 ^{o}C, for aluminum 1700 ^{o}C. For ablation, the required ion current density for ~ 300 keV ions is ~ 140 A/cm^2 assuming a 100 ns pulse duration. For higher energy the ion range in the material is greater and the required ion current density would be higher.

The results of detailed calculations for the dynamic temperature behavior of aluminum under the action of HPPIB are illustrated at **Fig. 1.**[14, 18] As it can be seen from these calculations, the melting temperature is reached for ion current densities j > 50 A/cm^2 and 100 ns pulse duration. The resolidification is near $6*10^9$ ^{o}K/s for ion beams of 180 keV and 150 A/cm^2 current density.

MPOS/ HPPIB technology

The final choice of the ion beam generation technology for material treatment is related directly with its commercial applicability - whether the technology employed for the generation of the beams is scaleable to large areas, is cost effective, is low in maintenance and user friendly. In this project we tested a novel approach for generation and application of ion beam, based on the technology of Microsecond Plasma Opening Switch.[15] In contrast to conventional high voltage vacuum or plasma filled ion diode technology used for generating high power pulsed ion beams, the MPOS approach is based on formation of the ion beam from the boundary of current carrying plasma during fast transition of the plasma from a conducting state to a high impedance state, which is accompanied with generation of a high voltage short pulse. There are several pronounced advantages of this technology when compared to the other approaches for thermal treatments of materials using high power ion beams [16]:

* In MPOS the sheath is multidirectional and can treat a sample with a complicated shape that has irregularities on a mm scale in contrast to conventional ion beam technology based on uni-directional ion flow, which can provide surface irradiation only along 'line of sight'.
* MPOS technology is more efficient in converting electrical energy to ion beam energy compared with conventional ion beam technologies.
* MPOS technology is less expensive, simple, and more reliable. There is no need for complicated external magnetic fields for diode insulation and large energy storage to power the field coils.
* MPOS technology could be easily scaled up to larger areas of treated surface, which is very difficult in case of conventional ion diode approach.

So, the advantages of the MPOS technique include: relative simplicity, combination of surface preparation and treatment in a single step, low up-front capital costs and low maintenance expenses.

MPOS Generator

The MPOS system differs from a pulsed ion diode approach in several important features: firstly, it uses a low voltage primary store of < 100 kV and does not need an external insulating magnetic field, which is mandatory in conventional PP ion diodes; and secondly, the HPPIB generated in the MPOS sheath is multi-directional and can treat a sample with a complicated shape that has irregularities on a mm scale. Another potential advantage of the MPOS approach is the

plasma that precedes the ion beam pulse. This plasma has a streaming energy of up to 100 eV and could provide 'degreasing' and initial preparation of the surface to be modified.

Our MPOS system is coaxial with a total inductance of 400 nH, and has the following parameters: charging voltage between 30- 50 kV, stored current up to 150 kA, rise time ≈1 μs, the load is either short circuit inductance or electron diode; the plasma source consists of 2 to 6 cable guns with variable charging voltage of 20-30 kV and variable rise time of 0.8-1.2 μs. The schematic of the device is given at **Fig. 2**[14]. The system uses standard electrophysical diagnostics for the MPOS parameters, and collimated Faraday cups with transverse magnetic field - to measure the density of the ion current along the cathode. The MPOS has demonstrated production of <100 ns ion beam of total up to 30 kA current over a surface area of about 200 cm^2 with an average energy of 150-200 kV. This corresponds to a voltage enhancement factor of 4-5. This represents a conversion efficiency of magnetically stored to an ion beam of about 25-30%.

Samples Preparation and Characterization

The materials used for the test samples were: 2024 Al alloy, 6061 Al alloy, 7075 Al alloy, stainless steel and carbon steels. The alloy compositions are listed in **Table 1**. The samples are flat with an approximate size of 20x20x2 mm. The surfaces of the samples were ground with sand paper from 240 grit to 600 grit and then were wet polished mechanically by using 0.3 μm α-Al_2O_3 micropolish. We also coated samples of aluminum with layers of either titanium, manganese or chromium of variable thickness from 160 nm to 500 nm. We also treated 6061 and 2024 5 mm thickness aluminum samples that had 2 x2 mm grooves machined into the surface to test the possibility of treatment of the surface with irregular shape. For fatigue studies the samples were made of standard shape with a neck, as it is shown in **Figure. 3** Conditions of HPPIB treatment of samples are given in **Table 2.**

Table 1. Alloy Composition of The Test Samples

Materials	Nominal composition, %
2024 Al	4.4- Cu, 0.6- .Mn, 1.5- Mg
6061 Al	0.6- Si, 0.28- Cu, 1.0- Mg, 0.20- Cr
7075 Al	1.6- Cu, 2.5- Mg, 0.23- Cr, 5.6- Zn
stainless steel	18-20 - Cr, 8-12 Ni, ≤0.08 C, ≤2.0 Mn, ≤1.0 Si
carbon steels	0.18-0.95 - C, 0.4-0.6 - Mn, ≤0.05 - P, ≤0.05 - S

Table 2. Processing Conditions for Ion Beam Treatment

materials	Al alloy, stainless steel, carbon steel
current density, j, A/cm^2	20-100
ion energy, E, keV	200-300
duration time, τ, ns.	60-100
shot number	3-10

Characterization of the surface properties was carried out using standard techniques. Microhardness was measured on the surface and cross-sections of the samples with a Buehler Micromet 2004 Microhardness Tester. Microstructure of the as-treated surfaces and the transverse cross-sections of the samples was observed with an optical microscope, an Axioplan with Zeiss optics, and a Philips EL30 Field Emission Scanning Electron Microscope with EDAX attachment. Composition of the samples with the thin films was determined using X-ray diffraction measurements by using a thin film attachment in a Siemens D5000 X-ray Diffractometer with a Cu target. We also used Auger spectroscopy for characterization of ion mixing in the pre-coated surface. The half-maximum peak broadening method was used to calculate the grain sizes of the treated surface layer. [17]

The tensile strength of the materials was determined according to American Standards ASTM E8M-88. A four-point bending fatigue test was used to determine the effect of ion beam treatment on the tensile and fatigue properties of the materials. The test arrangement is shown in **Fig. 3**. The load frequency was 30 Hz; the ratio of minimum load to maximum load was R=0.1. All fatigue data were collected with computer acquisition software. The maximum tensile stress is produced at the bottom surface of the samples and can be calculated following the formula: $S=3aP/(bh^2)$, where a is the distance from the sample support to the loading point; P is the maximum load; b is the width of the sample gauge length; and h is the thickness of the sample gauge length. The stress is constant between loading points for this scheme, which gives the possibility of corrosion measurements on this length.

The corrosion tests were done in a variety of ways. Simple tests were carried out by placing trea and untreated samples in 1% HCl solutions or 5% NaCl and 0.3% H_2O_2 solutions and then measuring relative mass loss. Anodic polarization curves were measured for the treated and untreated samples.

The corrosion fatigue measurements in the corrosive media were provided by immersing arrangement from the **Fig. 3** in the corrosion cell, maid from acrylic. This cell was filled by 0.5 M (about 3%) NaCl solution, which is close to sea water NaCl concentration.

II. Material Properties Study Results

Optical and SEM Studies

The optical and SEM pictures clearly showed that the microstructure of the ion treated region is much different from that of the untreated region. Melting of the surface was accompanied by pronounced changes in the surface microstructure and surface smoothing. A refined microstructure was obtained in the treated surface of the carbon steel sample, likely due to the rapid solidification of the surface melt. Significant change in the surface morphology was also observed on the treated surfaces of the stainless steel samples and the Al alloys. We have done grazing angle incidence diffractometer studies on treated and untreated samples. Some of the results indicate a decrease in grain boundary structure for the treated samples compared to the untreated ones. This is inferred from the fact that the width of the peaks in the diffractometer scans is increased for the treated samples. We have not been able to quantify the difference in grain sizes at this time.

The microstructure of the as-treated surfaces of the samples was observed with an optical microscope (OM) and a scanning electron microscope (SEM). Selected samples were then sectioned and mounted before grinding and polishing. The microstructure of the cross-sections was observed.

Formation of Craters

The typical micrographs of the as-treated surface of the samples are shown in **Fig. 4 a,b.** Craters were produced in the as-treated surface of carbon steel, stainless steel and various Al alloys samples using a current density of 60-100 A/cm^2. Craters were not observed in the as-treated surfaces of the samples with a current density of 40 A/cm^2 or lower. Typical ion beam energies used for the treatment of the samples were between 200 keV and 300 keV.

The density and mean diameter of craters measured on the as-treated surfaces of various samples are summarized in **Table 3.** It appears that the size distribution of craters is independent of the current density of ion beam. For ion energies of 200 t0 300 keV, most of the craters in the as-treated surfaces of the samples exhibit a diameter of about 10-20 μm and are uniformly distributed within the entire region of the treated surface. It was shown in related work [18] that the crater's sizes reach (1-2)10^2 μm diameter for ion beam 600 keV and 800 keV.

Table 3. The Density and Mean Diameter of Craters *

current density	density, craters/mm^2			mean diameter, μm		
A/cm^2	Al alloy	c steel	s steel	Al alloy	c steel	s steel
j ≤ 40	0	0	0	0	0	0
j = 60	40-60	760	930	16	15	18
j = 80	420-570	1330	1120	15	17	19
j = 100	780-840	1980-2460	1460	19	16	19

* ion energy = 200-250 keV

So, from this point of view a lower ion beam energy is preferable. The density of craters increases with increasing ion beam current density within the range of 40-100 A/cm^2. As the current density increases from 40 A/cm^2 to 100 A/cm^2, the crater density increases from zero to 780-840 craters/mm^2 for Al alloy samples and 2180-2460 craters/mm^2 for carbon steel samples.

Inspection of the micrographs reveals that all the craters appear to exhibit a circular geometry and the larger sized craters exhibit a multilayer structure with a depression in the center region surrounded by an outer layer. Several possible mechanisms for crater formation have been proposed and discussed earlier [19]. They include: 1)ion beam non-homogeneity; 2) contaminants with low melting and evaporation temperatures on the sample surface; 3) Unipolar arc formation on the sample surface; 4) absorbed gas extraction through the melting layer; and others. The present results suggest that the most likely cause is just the evaporation process because at low pressures (less than 10^{-4} Torr) evaporation begins immediately after melting.

Surface Melting

Evidence of surface melting was observed on the surfaces of the samples of various materials treated with a current density of 60-100 A/cm^2 and an energy of 200 -300 keV. Typically, energies of a few J/cm^2 are needed to heat and melt a surface layer of a few microns in thickness. The lowest energy density for the surface melting of the steel samples and the Al alloy samples in this study is about 1.2-1.6 J/cm^2, corresponding to an ion energy of 200 keV, a current density of 60-80 A/cm^2 and a pulse duration of 100 nanoseconds. The greater the ion energy then greater the energy density needed for melting, since the ion range in materials, and therefore the melting layer thickness, is nearly proportional to the ion energy.

Associated with surface melting is a significant modification of the surface microstructure. The microstructure of the treated region is distinctly different from that of the untreated region. A complex microstructure was obtained on the as-treated surface due to the rapid melting and solidification of the surface layer. It has been reported that in the case of carbon steel a complex nano-crystal structure of about 100-200 nm thick was formed on the treated surface of steel and is composed of ferrite (α-Fe) and austenite (γ-Fe) grains.[10] The results obtained from X-ray diffraction indicate that the grain sizes of the surface layer of the treated samples were greatly refined. The data for treated Al alloys are listed in **Table 4**. The respective typical X-ray diffraction patterns are illustrated at **Fig. 5**. All peaks in these figures are identified as of Al. However, the results gave only the order of magnitude. Since most alloy samples strongly absorb X-rays, the intensity of the incident beam is reduced almost to zero at a very short distance below the surface. The diffraction beams therefore originate chiefly from a thin surface layer, that is, some effective depth of X-ray penetration. This depth can be calculated from the following expression,

$$G_x = (1 - e^{-2\mu x/\sin\theta}) \qquad (1)$$

where G_X is the fraction of total diffracted intensity which is contributed by a surface layer of depth x. μ is the attenuation coefficient.[17]

Table 4. Grain Sizes of the Samples*

sample	2024 Al	6061 AL	7075 Al	carbon steel
untreated	28 μm	30 μm	25 μm	28 μm
treated layer	0.25 μm	0.5 μm	0.15 μm	0.036 μm

* ion beam energy = 250-300 keV, ion beam current density = 80-100 A/cm^2

In this study, the conditions applicable to equation (1) are $\mu = 135.684\ cm^{-1}$ for Al and $2\theta = 1°$. Using equation (1), a plot of G_x as a function of x indicates that 95 percent of the information from the diffraction pattern is contributed by the surface layer of about 1.0 μm depth, but 50 percent of this information originates from the first 0.2 μm depth of surface layer.

Examination of the cross-sections of the treated samples a scanning electron microscope reveal a change in microstructure from the treated surface layer to the untreated underlying region. The melting layer thickness estimated from SEM measurements is about 0.5 and 1-2 μm for steels and Al alloys, respectively. **Figure 6** shows an SEM of cross-sectioned Al2024-T3. Note that the upper 15 μm layer is nickel plating to facilitate cross-sectioning without damage to the modified surface layer.

Microhardness Measurements Results

The microhardness measurements on aluminum and different steels were done at the surface and on the cross-section versus depth using a load of 10 g. There was no discernible increase in the microhardness for all aluminum samples, which is typical for the Al alloys, and has been observed in other work on irradiation of aluminum with HPPIB.[5] The Al 6061 alloy includes about 1.2% of Mg. The solubility curve of Al-Mg system shows that with heating the Mg is not dissolved in the Al and the system hardness does not increase, i.e. Al 6061 microhardness and plasticity cannot be changed with thermal treatment. This agrees with our results. The slight decrease of the microhardness value could be related to the ion beam thermal relief of micro-stresses (generated by the polishing) just below the surface. A number of carbon steel samples with different carbon content and different initial microhardness were treated with ion beams of energy 250 keV and current density 80-110 A/cm^2. The results in this investigation have shown that for the shot numbers in the range of 4 shots to 10 shots the microhardness of the irradiated samples does not depend on the number of shots. Carbon steel hardness demonstrated significant increase after the ion beam treatment (2-3 times) , but stainless steel coupons HPPIB irradiation resulted in decrease of microhardness.

These results indicate that the microhardness changes are related with the initial conditions of the sample materials and their potential hardenability. It is possible that the surface layer of the stainless steel was post-annealed after being treated with ion beams, resulting in a decrease in the microhardness. In the case of carbon steel samples, some martensite phase is formed on the surface layer due to the rapid melting and solidification during the ion bombardment, producing higher microhardness [10].

The microhardness of the treated carbon steel coupons as function of the carbon abundance is plotted in **Fig. 7.** The results showed that the microhardness of carbon steel after HPPIB treatment increased with increase of carbon abundance, and higher values of microhardness were obtained for the pre-hardened samples.

The values of the microhardness for the treated surfaces of the carbon steels are related to the current density of the ion beams. With an increase of current density in the range of 40-100 A/cm^2, the microhardness increases for carbon steel samples (both non-hardened and pre-hardened) as shown in **Fig.8.** A significant change of the microhardness is observed when the current density of ion beams is in the range of 60-80 A/cm^2.

We also tried to measure microhardness along the cross-section of the samples as function of depth from the surface. But the low accuracy of placing the load bearing tip (which provided the width of the indetation of 1-2 microns in size) seriously limited the value of the obtained results. Therefore our data on microhardness measurements are likely to be underestimated, and it is more appropriate in this case to use nano-indentation techniques. A significant change of microhardness was registered for the carbon steel sample with higher value at the treated surface and for the stainless steel sample with lower value at the treated surface. The sharp changes are limited to the treated surface region of the ion beam affected layer which is on the order of a few microns. **Figure 9** shows some results for microhardness versus depth from the material surface.

In the case of Al alloys samples the observed changes in microhardness on the cross-sections are not significant and a slight change within the range of 30 HV was measured. These results suggest that the ion beam treatment produced limited influence on the microhardness of the Al alloy samples in this study.

Corrosion Tests Results

A weight loss method was used for the corrosion test of the 2014, 6061 and 5083 Al alloy samples. A solution of 1% NaCl was used for 5083 and 2014 Al alloy samples, and a solution of 55 NaCl and 0.3 H_2O_2 - for 6061 Al alloy sample. The treated and untreated samples were immersed in the solution separately and the weight loss was measured after 24 hours and 48 hours. The results of corrosion tests for Al 5083 and Al 6061 alloy samples are given in **Table 5.** Typically all ion beam irradiated samples show a decrease in mass loss of up to 2-3 times and more [20].

Table 5: Weight Loss of the samples

Sample	Weight Loss (mg / cm^2)			
	24 hrs.		48 hrs.	
	untreated	treated	untreated	treated
5083 Al	1.7	1.5	36.8	13.3
6061 Al	6.8	2.7	16.3	6.6

DC anodic polarization measurements were done for treated samples of Al 6061 and Al 2024 in a solution of 1% NaCl. The results of these measurements are given in Figure 10. The current amplitudes for the ion-treated samples compared to that for the untreated are a factor of 2.5 to 3 lower. This is also in reasonable agreement with the mass loss corrosion measurement.

Corrosion Tests on Irregular shaped Samples and Long Strips of Aluminum

We also tested if the ion beam treatment from our system is multi-directional in nature and not 'line of sight' as in vacuum PP ion diodes. Because the plasma density in our system is high enough to generate sheaths with thicknesses of a few mm ($10^{14\text{-}15}$ cm^{-3}) we surmised that the ion beam, extracted from the plasma, would be capable of treating objects that are not flat but have surface irregularities on this scale size. In order to demonstrate this we took 2024-T3 aluminum alloy 5 mm thick and machined 'slots' of 2 mm depth to provide side surfaces normal to the axis of the cathode. The piece was masked so that one half was covered and would not be treated by the ion beam. After treatment and corrosion for a 24 hour period, the side surfaces of the sample, that were left exposed to the ion beam for treatment suffer much less corrosion than the similar untreated sides. Although this is not a particularly quantitative test, it is clear that the MPOS technology can treat surfaces that are irregular in shape. We also wanted to address the issue of the maximum sample size that could be treated by our system. We placed a strip of 6061 aluminum about 12 cm in length along the cathode shank. The strip was held to the cathode with copper tape in several places, which prevented the ion beam treatment at tape locations. After exposure to the ion beam we placed the Al strip in 1% solution of HCl and left it for 24 hours. The results clearly showed the enhanced corrosion resistance for the portions of the strip, which were treated with a wide range of the ion current density 40-100 A/cm^2.

III Ion Mixing with HPPIB

There is an increasing number of investigations on corrosion and adhesion enhancements by ion beam mixing for various combinations of thin film and substrates [21]. It is well-known that adhesion is one of the most important factors determining the degree of chemical attack like corrosion on the film/substrate system. The cause for bad adhesion is sharp boundary between film and substrate for all traditional methods of the thin film deposition. To improve the adhesion, many attempts have been made by using ion bombardment to create the intermixed layer between film and substrate. Although many studies have been carried out on low current ion bombardment (ion implantation) where the mixing is due to collisional and radiation diffusion effects (see, for example [22-24] , only few studies have been reported for high power pulsed (HPPIB) ion beam mixing which is occurred due to fast melting of the surface layer and convective mixing[25]. HPPIB treatment of surfaces is a thermal process that does not significantly alter the atomic composition of the sample. The implanted ion concentration, over the ion range in the sample, is typically less than 10^{-3} atomic percent. We tested MPOS/HPPIB approach for preparing Ti/Al films with ion mixing at the boundary. Single layer 500 nm films of titanium were deposited on aluminum alloy 6061-T6 samples. The films used in these studies were deposited using a four hearth electron beam evaporator. The thickness of the evaporated films were measured using a Tencor Alpha-Step 200 profilometer. Characterization of the treated samples was done using the SEM, EDAX and Auger spectroscopy. The EDAX analysis was done as a function of electron beam energy for energies between 5 kV and 30 kV, the maximum beam energy of the SEM. A comparison of the results of the EDAX analysis for treated and untreated parts of the same sample, as a function of electron beam energy, can give a qualitative picture of the composition of the sample as a function of depth since the electron beam range in the sample is a function of energy. The higher the electron beam energy, the longer the range in the sample and therefore, the deeper the sample is probed. We could plot percent composition of a given element, for both treated and untreated sides of the sample, versus electron range by estimating the range in the sample. A comparison of the plots was an indication of whether mixing occurred. If it seemed likely that the treatment caused some mixing then we had an Auger spectrum done.

Computer Simulation on HPPIB Interaction with Surface

For estimation of the ion current density needed for the effective melting and mixing of the films and substrate the numerical calculations of the phase transitions in this system have been

done. These calculations were carried out using the numerical model BETAIN [26] This model is used for the interaction modeling of high power electron and ion beams that have various shape of energy spectrum and current pulse Vs time with planar sample surfaces (one- or multi-layered). The calculations were done for the measured parameters of the HPPIB generated by our MPOS system. **Fig. 11** shows the dependence of the melted and evaporated layers thickness from the ion current density. The difference between these two values gives the estimation of the layer thickness where the mixing occurs. For ion current density of 150 A/cm^2 it gives $\delta \approx 1.1$ μm. As can be seen from these simulations, the most preferable ion current densities lies between 120-150 A/cm^2. Below this range the melted layer thickness is small and at higher ion current densities the thickness of melted layer increases very slowly because main part of the ion beam energy goes to the material evaporation.

Experimental results

The high voltage pulse amplitude was about 200-250 kV. Due to the fact that the ion current density changes from 10 to 150 A/cm^2 (it corresponds to 1.5 J/cm^2 energy input) along the MPOS on the length of 20 cm, we could treat samples with various current density by locating them in the different cathode positions. Four shots for the sample usually were provided to avoid influence of the some ion beam non-homogeneity. Part of the each sample was masked before irradiation to compare characteristics of the treated and untreated surfaces.

The best results in mixing were obtained at the voltage 250 kV and maximum ion curent density available on our installation j=150 A/cm^2, and all analysis discussed below were done for this case. The SEM micrographs show the significant surface smoothing for the treated samples in comparison with the untreated ones (**Fig. 12**) [27]. We also measured the microhardness of the Al6061-T6 substrate before deposition of the titanium film, after deposition and then after irradiation using the ion beam. The microhardness of the treated side of the sample was slightly lower than the untreated side of the sample. The microhardness of the aluminum substrate was about 50% lower than the treated or untreated part of the sample. **Table 6** shows the results. The simple corrosion test has been done by the immersion treated and untreated samples in 1% HCl solution. After 24 hours the Ti film on the untreated sample was totally removed and a severe pitting was observed on the substrate surface, but no change was observed for the treated samples. **Fig. 13** shows the Ti content measured by EDAX with the various probe electron beam energies for the treated (at 150 A/cm^2) and untreated samples. The curve for the untreated Ti/Al surface reveals the monotonous decreasing with the energy increase , but for the treated sample we have

slightly bell-shaped curve which indicates that Ti content reaches maximum on some distance from the surface. It is quite difficult to get the elements distribution through the depth from the EDAX measurements (it need solving of the reverse problem with enormous amount of parameters) but two obvious useful conclusion can be made: 1. The ratio of the total amount of Ti for the treated sample to the initial amount of Ti is not less than the ratio of contents at E=30 keV on the Figure 4. , which is about 0.75. So, Ti layer was not simply evaporated. 2. The Ti content on the treated surface is quite small. **Fig. 14** shows an Auger profile for the treated part of this sample. It indicates that significant mixing occurs to depth of 1.2-1.3 μm which is in reasonable agreement with numerical calculations (1.1 μm). The total amount of Ti for the treated sample is about 80 percent of the initial amount and it almost corresponds to the calculated value of the evaporated layer thickness (100 nm) from the initial 500 nm (see **Fig. 12**). It also corresponds good enough to the estimation from the EDA measurements (75%) The carbon and oxygen are likely due to the plasma constituents and surface layers.

Table 6. Microhardness measurements for the 6061-T6 aluminum without titanium, with a 500 nm thick titanium layer and after treatment.

Material	Al6061	500 nm Ti/Al6061	Treated Ti/Al6061
Hμ, kg/mm^2	110	160	150

Summarizing this paret of the experimental efforts, we:

- demonstrated the application of MPOS technology for ion beam mixing. The approach has specific features which give it advantages in comparison with the usual ion beam treatment.
- MPOS treatment provides the significant mixing of the 500 nm Ti film/Al substrate to the distance more than 1 μm.
- Experimental value of the mixed layer thickness corresponds to the numerical calculations.
- The treated mixed layer reveals improved corrosion properties.

This particular experiment substantiates the potential for MPOS/HPPIB system application for various film/substrate systems, including ceramics and semiconductors.

IV Al Alloys Bulk Fatigue Studies

Our previous experiments using MPOS/HPPIB have demonstrated that this treatment can significantly improve corrosion properties of various materials [20,27] It was shown that MPOS treatment provides 3-10 fold enhancement of corrosion properties of Al7075-T6, Al2024-T3, Al6061 alloys and has some advantages compared to the conventional high voltage vacuum diodes. But fatigue properties for these Al alloys after the ion beam treatment were not investigated before. It is well-known, however, that fatigue is the predominant type of failure for Al structures and, therefore, of primary importance. For all industrial applications, especially for aircraft, a reduction in the fatigue properties after treatment is not acceptable. It is well-known, also, that fatigue strength depends considerably on the surface condition. Rather small surface defects (few microns in depth) cause large reductions of fatigue strength compared to that for polished specimens [28]. Another very important fact is that fatigue strength of aluminum alloys is significantly lower in a corrosive medium than in a noncorrosive one, especially under low stresses for longer periods [29]. This effect is more pronounced for high strength Al alloys (2024 and 7075 series). According to data in [29] the axial fatigue limit for these alloys is 3-4 times lower in sea water than in air. The ion beam treatment obviously changes the surface condition, so the fatigue properties can be changed too. Therefore, from our point of view, the fatigue measurement after HPPIB treatment appears to be a necessary step in investigation of the Al alloys modification. This part of the final report is devoted mainly to the systematic measurements of the bending fatigue lifetime for Al2024-T3, Al7075-T6 alloys in air and in 0.5 M NaCl aqueous solution.

Materials and bending fatigue test technique

The materials used for the test samples are Al2024-T3 Alclad (4.4% Cu, 0.6 Mn, 1.5 Mg) and Al7075-T6 (1.6% Cu, 2.5 Mg, 0.23 Cr, 5.6 Zn). The sheet material with 1.6 mm thickness was used for both alloys. The processing parameters for the ion beam treatment of these samples were ion energy E=200 keV and the ion current density between 60 to 100 A/cm^2.

Experimental results

No difference was revealed for treated and untreated samples for both Al2024 and Al7075 alloys with ultimate tensile strength of 460 and 615 MPa respectively. This is understandable since the tensile strength is predominantly a bulk property of the material and the ion beam treatment

depth does not exceed a few microns in our case [3?]. Then the fatigue S-N curves (stress vs. number of cycles to failure) were measured.

Measurements in air.

S-N curves were measured for untreated samples and for samples treated with current densities of 60, 80 and 100 A/cm^2 for both alloys. For Al2024 the obtained S-N curves were practically the same for untreated samples and samples irradiated with current density 60 A/cm^2. For samples irradiated with ion current densities 80 and 100 A/cm^2 the fatigue lifetime was about 30-40 % more than for untreated ones at the higher stress levels (between 340 to 410 MPa). The Al 2024 S-N curves for untreated samples and samples treated with ion current density 100 A/cm^2 are given in **Fig. 15**. Another positive result for the Al2024 samples treated with 100 A/cm^2 is that statistical deviation from sample to sample is considerably less than for the untreated ones.
For Al7075 the obtained S-N curves were practically the same for untreated samples and samples irradiated with current densities between 60 to 100 A/cm^2 for the testing in the atmospheric air.

Measurements in 0.5 M NaCl aqueous solution.

Figure 16 shows S-N curves for Al7075-T6 samples, obtained in the corrosion cell, for untreated and treated with ion current density of 80-100 A/cm^2. The solid line at the top of this picture represents curve measured in air (statistically the same for treated and untreated samples).
For all stresses the fatigue lifetime is about two times more for the treated samples compared to the untreated ones. The fatigue limit at 10^7 cycles is 135 and 87 MPa for treated and untreated samples, respectively (note that in air it is about 300 MPa).

Figure 17 shows S-N curves for Al2024-T3 samples , obtained in the corrosion cell, for untreated and treated with ion current density of 80-100 A/cm^2. For Al2024 the MPOS treatment effect on the corrosion fatigue is not so pronounced as for Al7075. The behavior of the S-N curves for Al2024 is qualitatively similar in air and in corrosion media: at the higher stress levels the lifetime for treated samples is about 30-40 percent more than for untreated ones. This region lies above 340 and 240 MPa for air and NaCl solution, respectively. The fatigue limit at 10^7 cycles in the corrosion solution is slightly higher for treated samples in comparison with the untreated ones

(113 and 103 MPa) respectively. The small influence of the MPOS treatment for the Al2024 fatigue property at low stresses can be associated with the already high corrosion resistance of the surface layer for the Alclad material. The detailed information on fatigue and corrosion fatigue measurements for Al2024-T3 Alclad and Al7075-T6 alloys substantiates improvement in respective properties for Al7075-T6 after the MPOS treatment. For Al2024 some enhancement of the fatigue life time was also documented for higher loading operation conditions.

Programmatic Plans and Milestones

First year goals

- Design and fabrication of experimental system **Completed**
- Testing and characterization of the experimental system **Completed**
- Scaling study of HPPIB treated steel samples for microhardness enhancement **Completed**
- Scaling study of HPPIB treated Al samples for corrosion resistance **Completed**

Second year goals

- Scaling study of variation of tensile bulk properties of HPPIB treated Al alloys samples **Completed**
- Scaling study of fatigue bulk properties of Al alloys samples **Completed**
- Demonstration of ion mixing with enhanced corrosion properties **Completed**

References

[1] Microstructure of Irradiated Materials, eds. I.M. Robertson, L.E. Rehn, S.J. Zinkle and W.J. Phythian, MRS Symposium Proceedings, vol. 373(1995)

[2] J.K. Hirvonen, Annual Review of Materials Science, 1989, vol. 19:401-417

[3] G.E. Remnev and V.A. Shulov, Laser and Particle Beams, 1993, vol. 11(4):707-731

[4] A.D. Korotaev, A.N. Tyumentsev, Y.I. Pochivalov and S.V. Ovchinnikov, Physics of Metals and Metallography, May 1996, vol. 81(5):542-548

[5] Z.W. Kowalski, Journal of Materials Science, July 1994, vol. 29(13):352-355

[6] H.A. Davis, G.E. Remnev, R.W. Stinnett and K. Yatsui, MRS Bulletin, Aug. 1996. vol. 21(8):58-62

[7] Z.G. Shen, C.H. Lee, C. Wu and D.Y. Jiang, Journal of Materials Science, July 1990, vol. 25(7):3139-3141

[8] E. Mccafferty, P.M. Natishan and G.K. Hubler, Corrosion Science, 1993, vol. 35(1):4239-4246

[9] L.G. Romanov, I.N. Tsareva, A.D. Pogrebnyak and G.M. Romanova, Journal of Friction and Wear, 1992, vol. 13(5):90-96

[10] V.I. Itin, Y.F. Ivanov, S.V. Lykov, G.A. Mesyats, G.E. Ozur, D.I. Proskurovsky andV.P. Rotshtein, Proceedings of 9th International Conference on High-Power Particle Beams, vol. III:1942-1947, Washington DC, 1992

[11] Surface Modification and Alloying by Laser, Ion, and Electron Beams, eds. J.M. Poate, G. Foti and D.C. Jacobson, 1983, Plenum Press, N.Y.

[12] M.D. Gabovich, N.V. Pleshivtsev and N.N. Semashko, Ion and Atomic Beams for Controlled Fusion and Technology, Consultants Bureau, New York, 1989

[13] Handbook of Ion Beam Processing Technology, ed. J.J. Cuomo, S.M. Rossnagel and H.R. Kaufman, Noyes Publications, 1989

[14]. V. Bystritskii, Y. Yankelevich, E. Garate, A. Kharlov, et. al., Modification of Material Surface with Plasma Enhanced Ion Beams, IEEE 11-th International Conf. on Pulsed Power, Baltimore, Maryland, June 29-July 1997, p. 296

[15] Bystritskii, V.M.; Mesyats, G.A.; Kim, A.A.; Koval'chuk, B.M.; and others. Microsecond plasma opening switches]. Fizika Elementarnykh Chastits i Atomnogo Yadra, Jan.-Feb. 1992, vol.23, (no.1):19-57.
Translation: Soviet Journal of Particles and Nuclei, Jan.-Feb. 1992, vol.23,

[16] V. Bystritskii, S. Grigoriev, I. Lisitsyn, et.al., Proc. IEEE 9-th Intern. Confer. on Pulsed Power, Albuquerque, NM, 1993, v. 2, p. 1013

[17] B.D. Cullity, Elements of X-ray Diffraction, 2nd ed., Addison-Wesley Publishing Company, Inc., 1978, p.257-272

[18] V.M. Bystritskii, P.V. Burkov, S.V. Grigoriev, A.V. Kharlov, A.A. Sinebryukhov, Theoretical and Applied Fracture Mechanics, 1997, Vol. 26, No. 2, p. 151.

[19] A.D. Korotaev, G.E. Remnev et al., Physics of Metals and Metallography, 1996, No.5, p. 542.

[20] Bystritskii, V.M.; Yankelevich, Y.B.; Kharlov, A.V.; Garate, E.; and others. Plasma-ion beam treatment of Al for enhanced corrosion resistance: IEEE International Conference on Plasma Science, San Diego, CA, USA, 19-22 May 1997, New York, NY, 1997, p. 119

[21]. G.K. Wolf, W. Ensinger, Nucl. Instr. & Methods, B59/60, 1991, p. 173.

[22]. J.E. Baglin, IBM Journ. of Res. and Development, v. 38, # 4, 1994, p. 413.

[23]. D.L. Santos, J.P. Souza, et.al., Nucl. Instr. & Methods, B103, # 1, 1995, P. 57.

[24]. H. Hasyama, Y. Shima et.al., Nucl. Instrum. & Meth. B80/81, # 11, p. 1304

[25]. V. Grigoriev, T. Koval, et.al., In Proc. All Russian Confer. on Material Modification, 1996, Tomsk (in Russian) , p. 213.

[26]. V. Val'chuk, S. Khalikov, A. Yalovets, Mathematical Modeliing (in Russian) , v. 4, n. 10, 1992, p. 111.

[27]. V.M. Bystritskii, E. Garate, A. Kharlov, E. Lavernia, et al., Proc. Pulsed Power conference., Baltimore, USA, 1997, p. 1054.

[28]. M.L. Sharp, G.E. Nordmark, C.C. Menzemer. Fatigue design of aluminum components and structures, 1996, NY, p. 108-110.

[29]. E.H. Hollingsworth, H.Y. Hunsicker, In Book: Corrosion and corrosion protection handbook, edited by Philip A. Schweitzer, 1983, p.135-137.

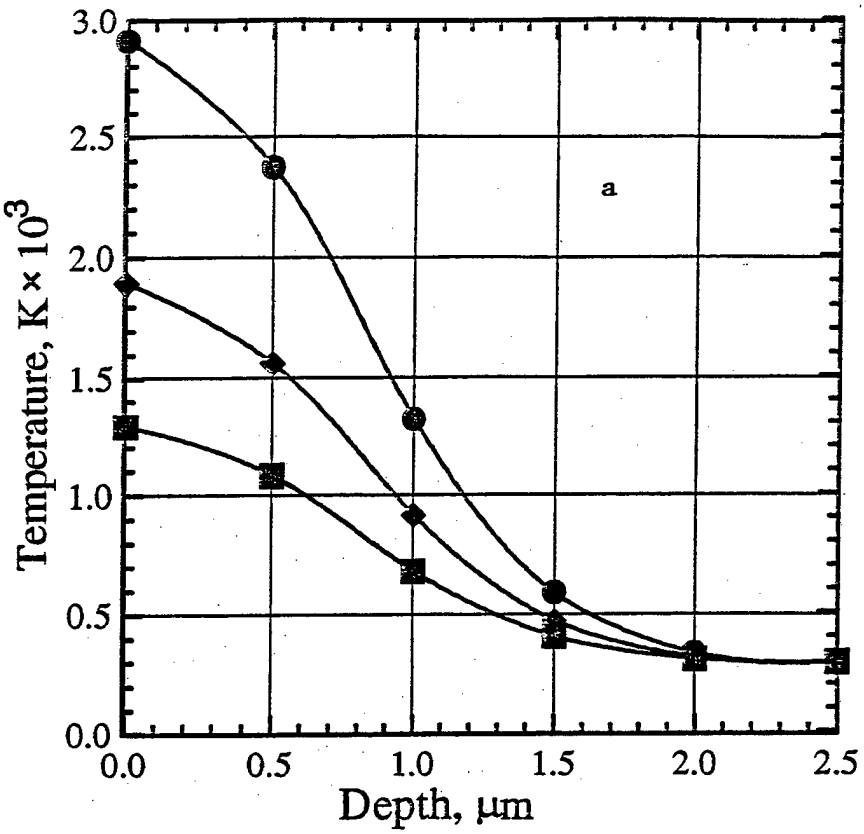
3.0
2.5
2.0
1.5
1.0
0.5
0.0
Temperature, K × 10^3
a
0.0
0.5
1.0
1.5
2.0
2.5
Depth, μm

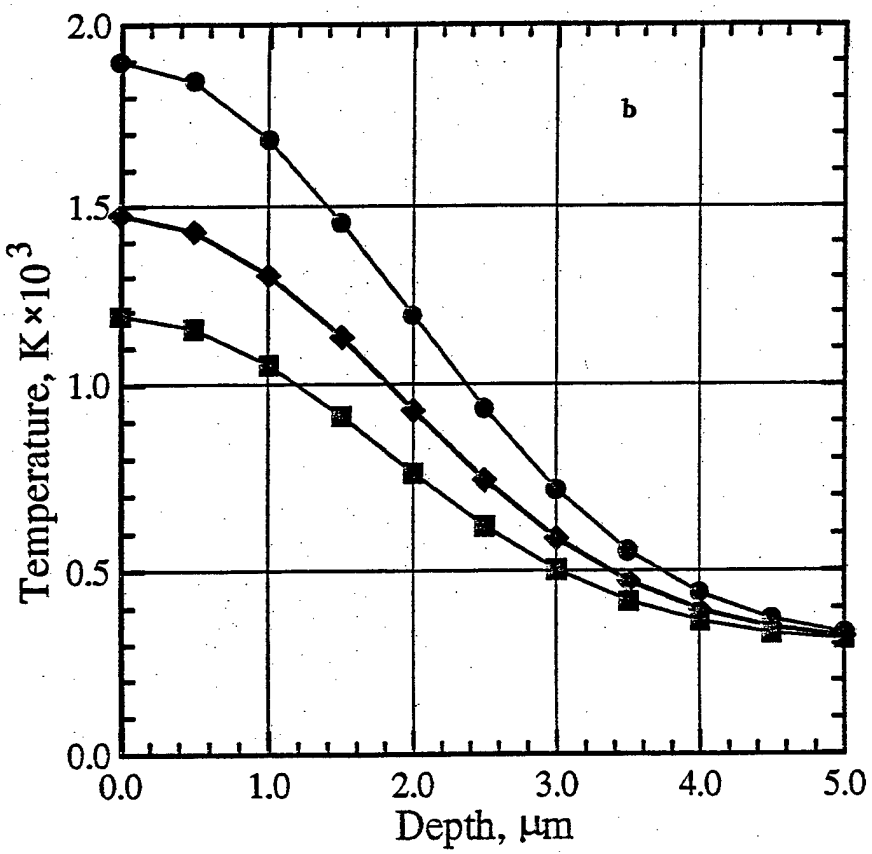
2.0
1.5
1.0
0.5
0.0
Temperature, K ×10^3
b
0.0
1.0
2.0
3.0
4.0
5.0
Depth, μm

FIG. 1

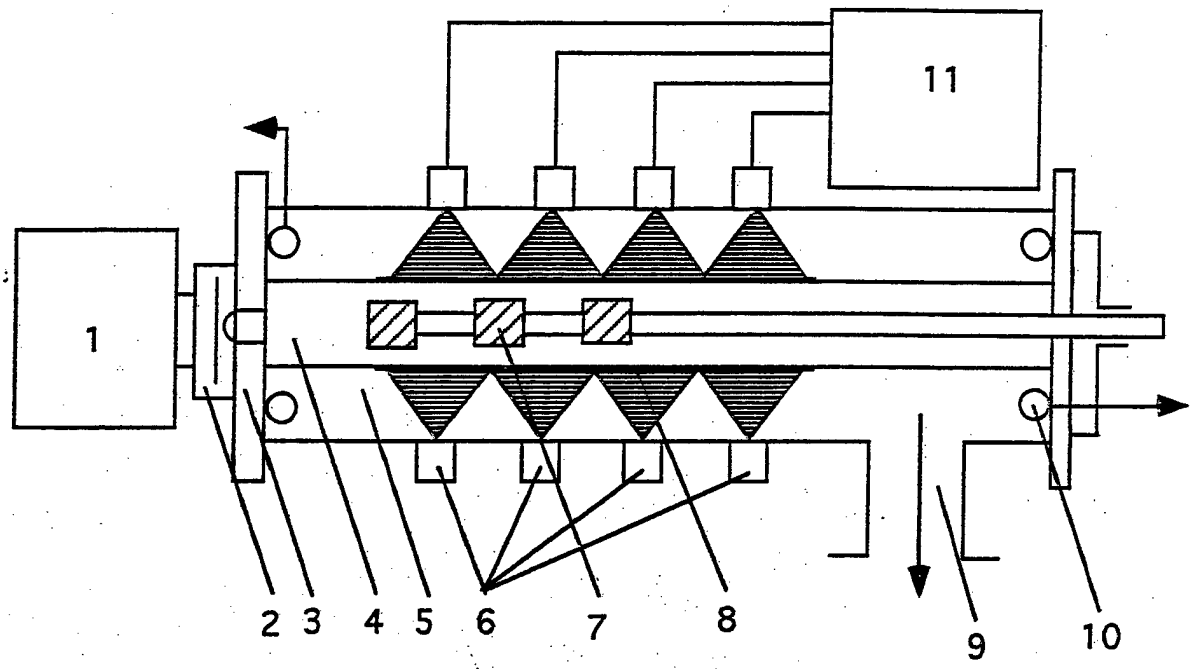

1. Primary energy source
2. Gas pressurized spark gap
3. Insulating vacuum interface
4. Cathode electrode
5. Anode electrode
6. Plasma guns
7. Ion diagnostics
8. Material samples
9. Pumping port
10. Current diagnostic
11. Power supply for plasma guns

FIG. 2 Schematic of the HPIB System

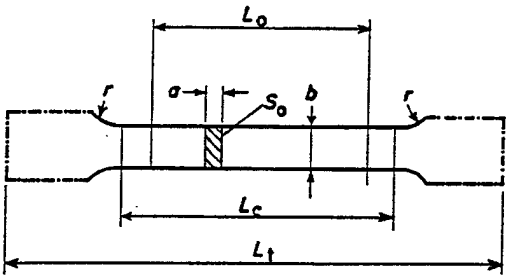

FIG. 3 Dimension of The Rectangular Sample(American Standards ASTM E8M-88)
b = 6.0 mm, L_0 = 25 mm, Lc = 32 mm, r = 6 mm, Lt = 100 mm

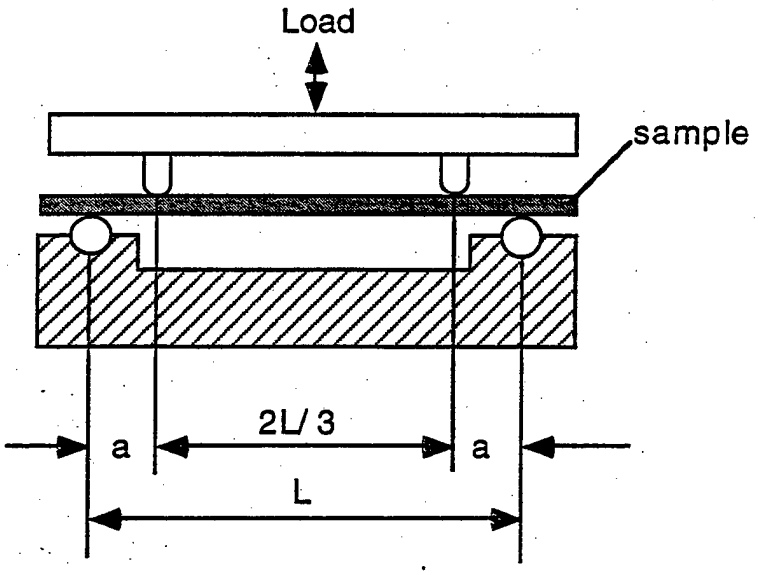

FIG. 3 Sample Arrangement for Four-Point Bending Fatigue Test
L = 45 mm, sample width b = 2.5-4.1 mm, thickness h = 1.5-1.6 mm

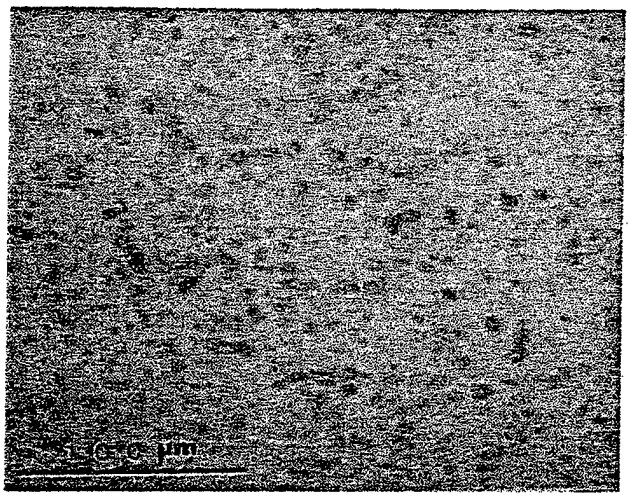

$j = 100\ A/cm^2,\ E = 200\ KeV$

FIG. 4 a Surface structure of ion beam treated carbon steel

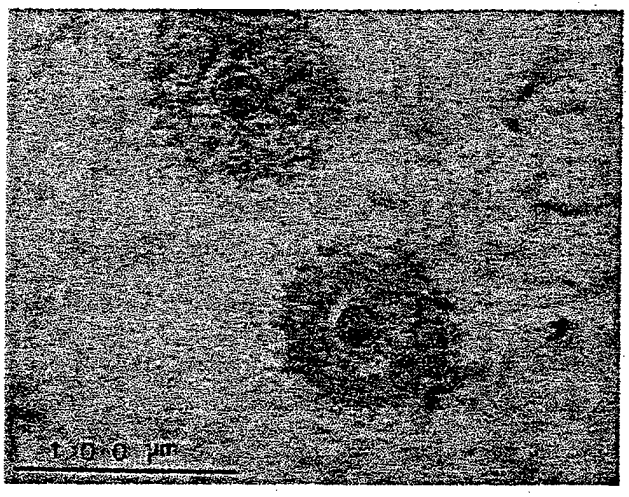

FIG. 4 b Surface structure of ion beam treated 6061 Al
$j = 80\ A/cm^2,\ E = 200\ KeV$

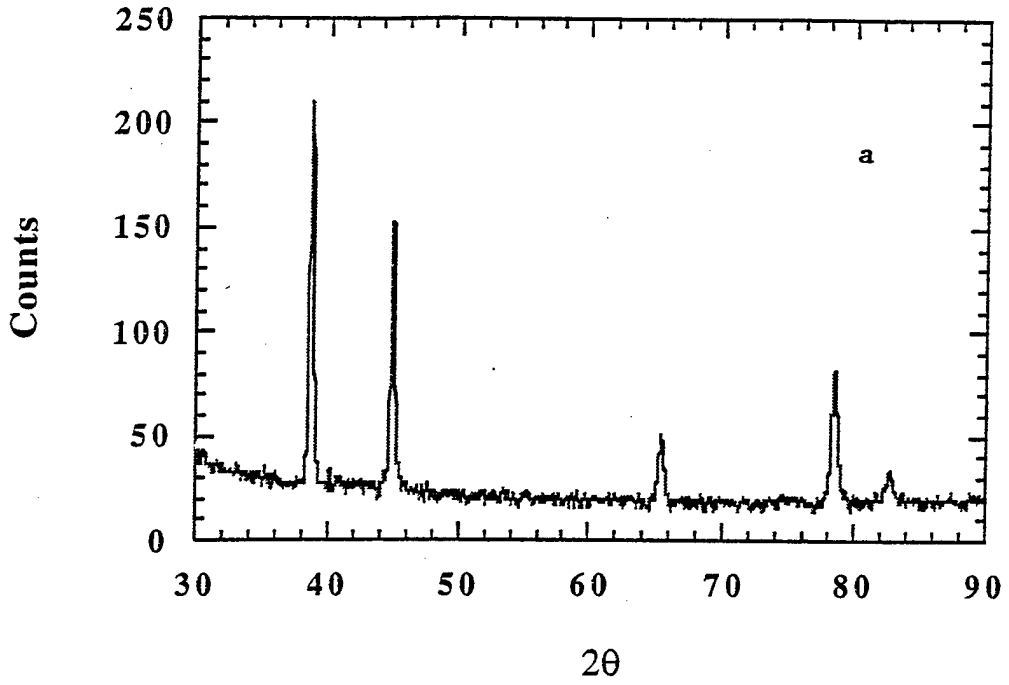

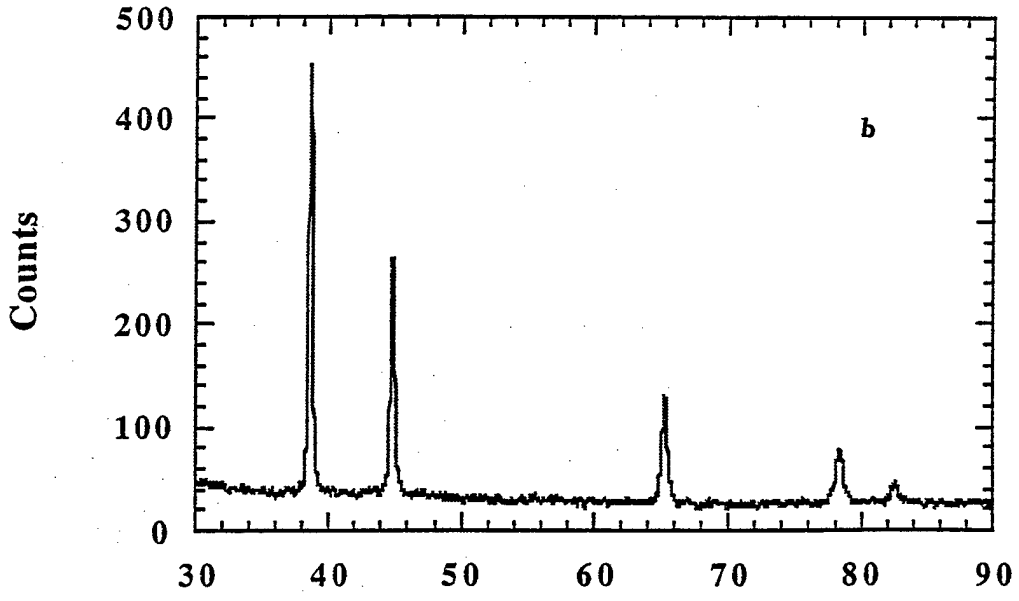

FIG. 5 X-ray diffraction patterns from 2024 Al samples

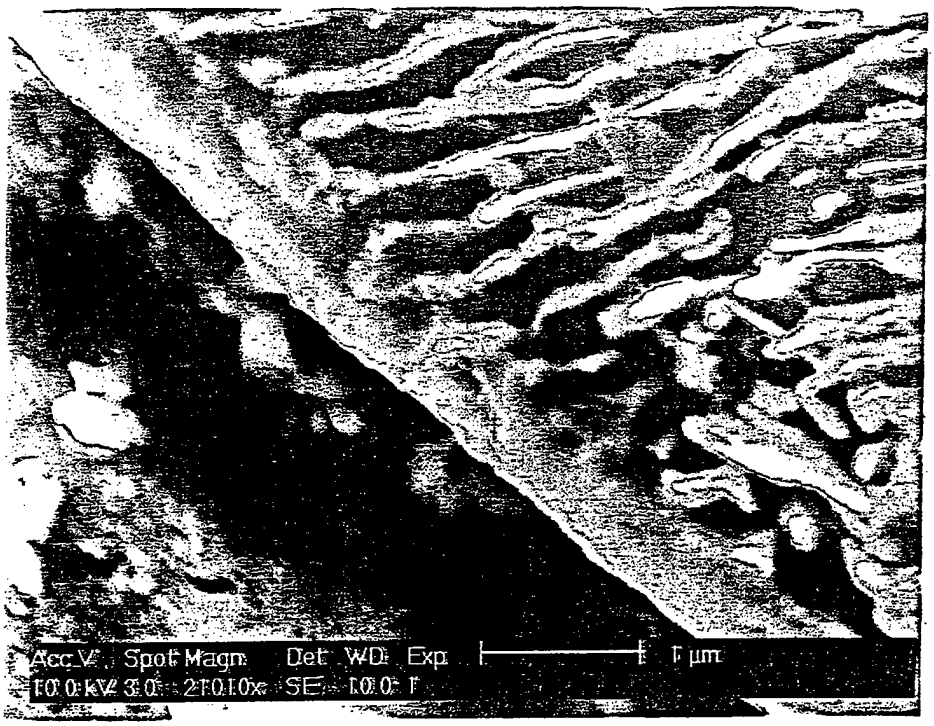

FIG. 6

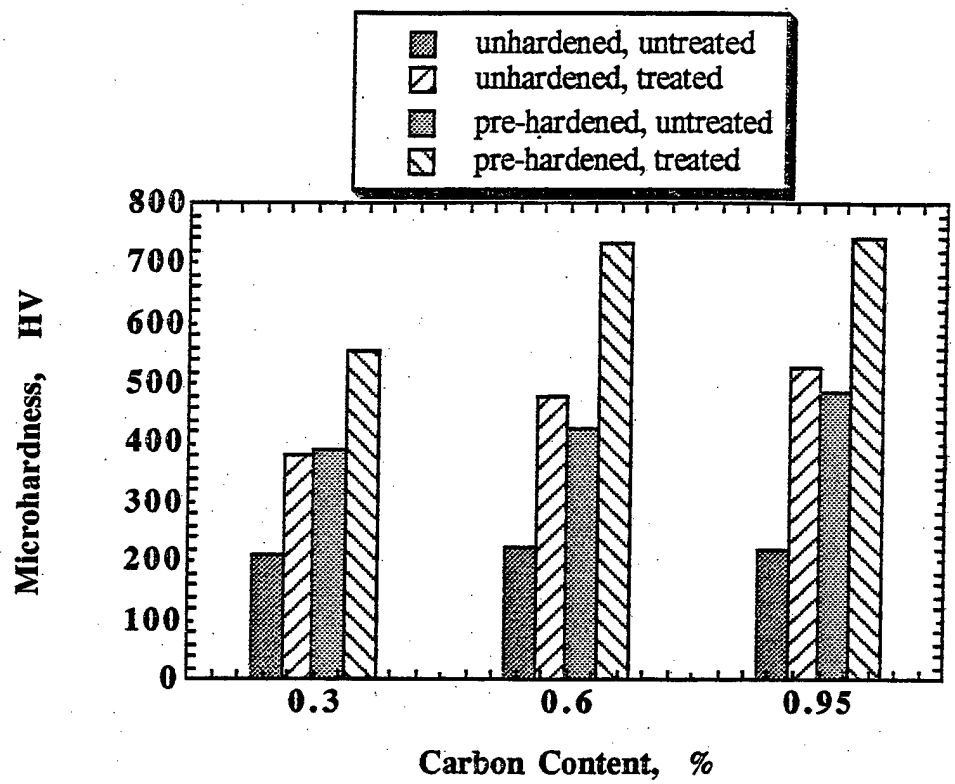

FIG. 7 Microhardness of carbon steel samples with different carbon content treated with j = 80-110 A/cm^2, E = 250 KeV,

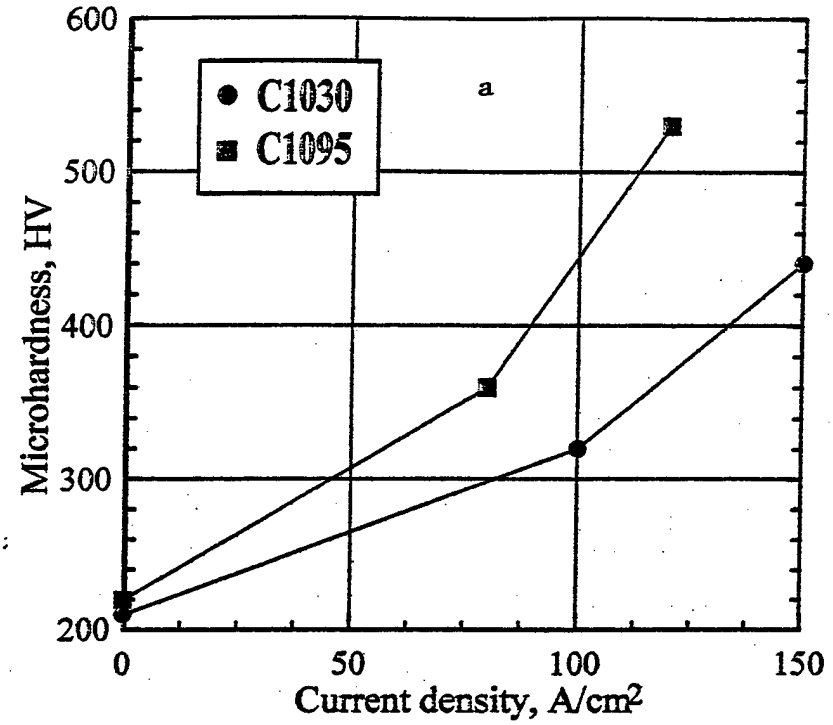
600
500
400
300
200
Microhardness, HV
C1030
C1095
a
0
50
100
150
Current density, A/cm2

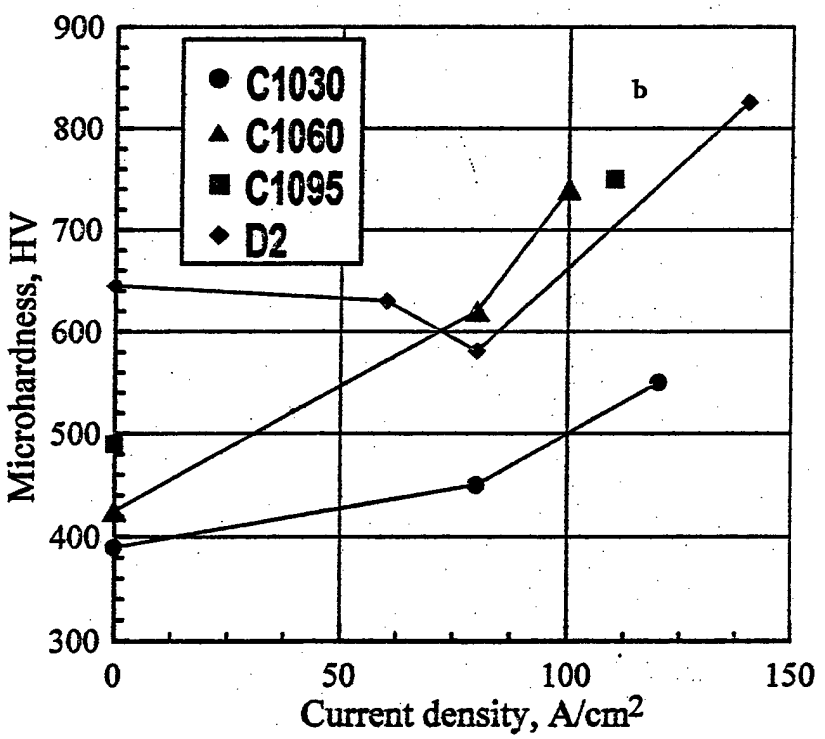
900
800
700
600
500
400
300
Microhardness, HV
C1030
C1060
C1095
D2
b
0
50
100
150
Current density, A/cm2

FIG. 8

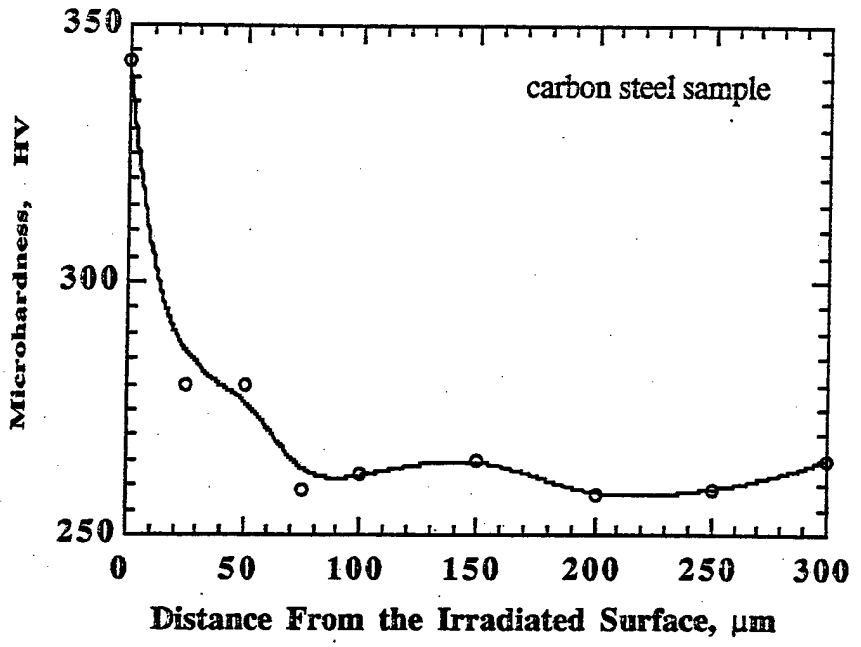

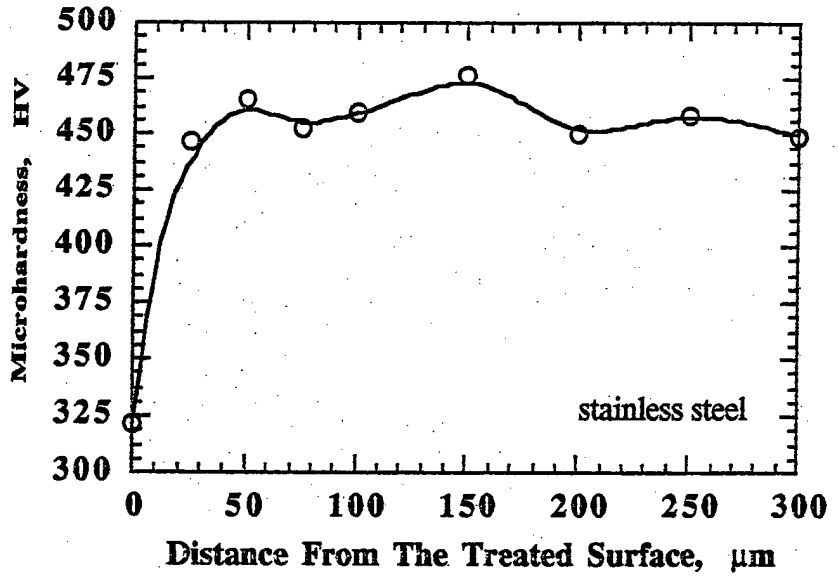

FIG. 9 Microhardness on the cross-sections of carbon steel and stainless steel samples

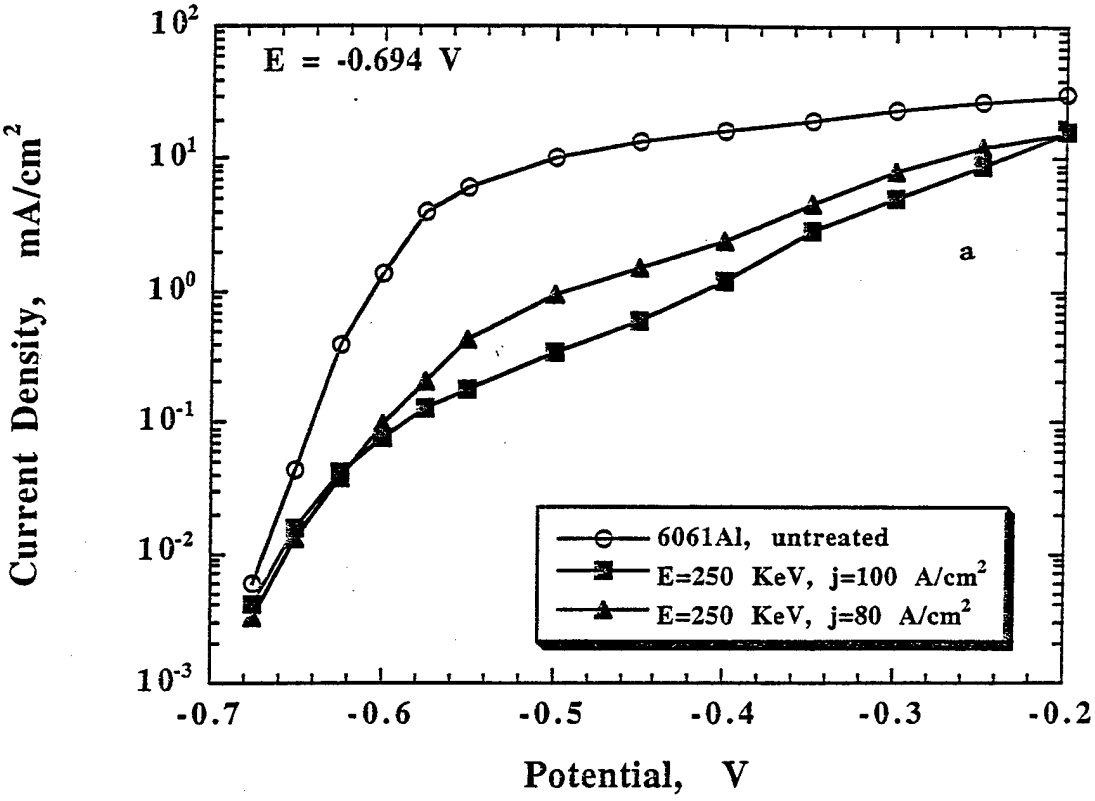

FIG. 10 Anodic polarization curves for 6061 Al alloy samples

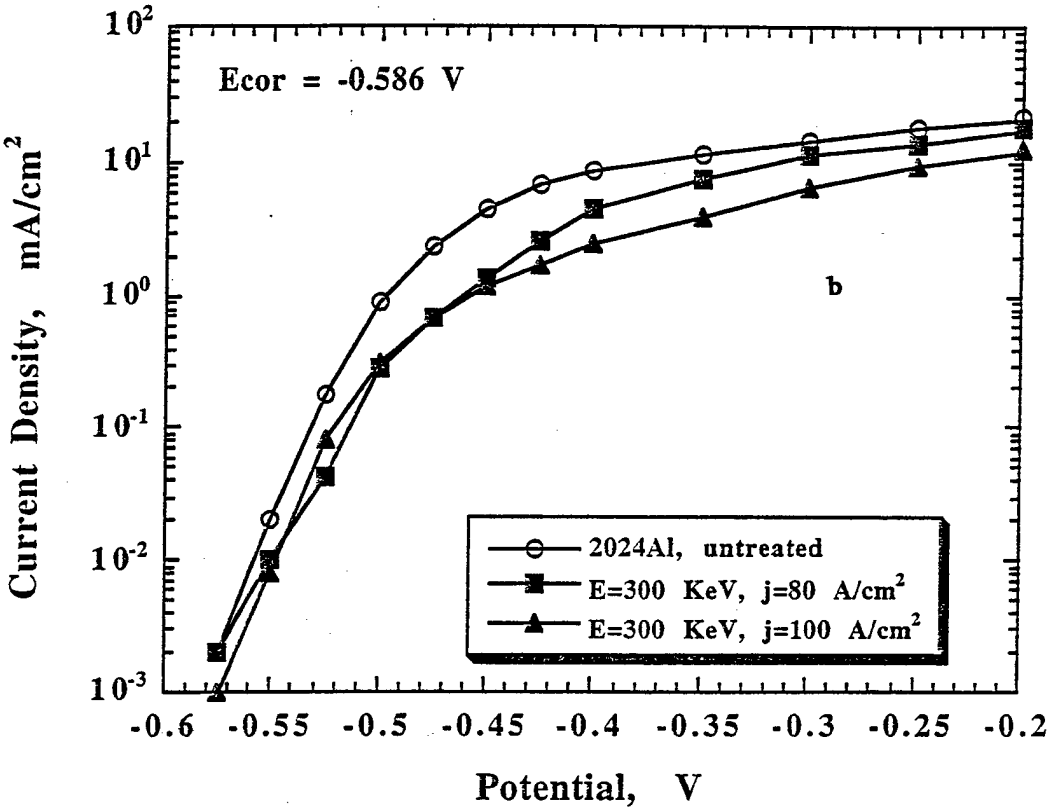

FIG. 10 Anodic polarization curves for 2024 Al alloy samples

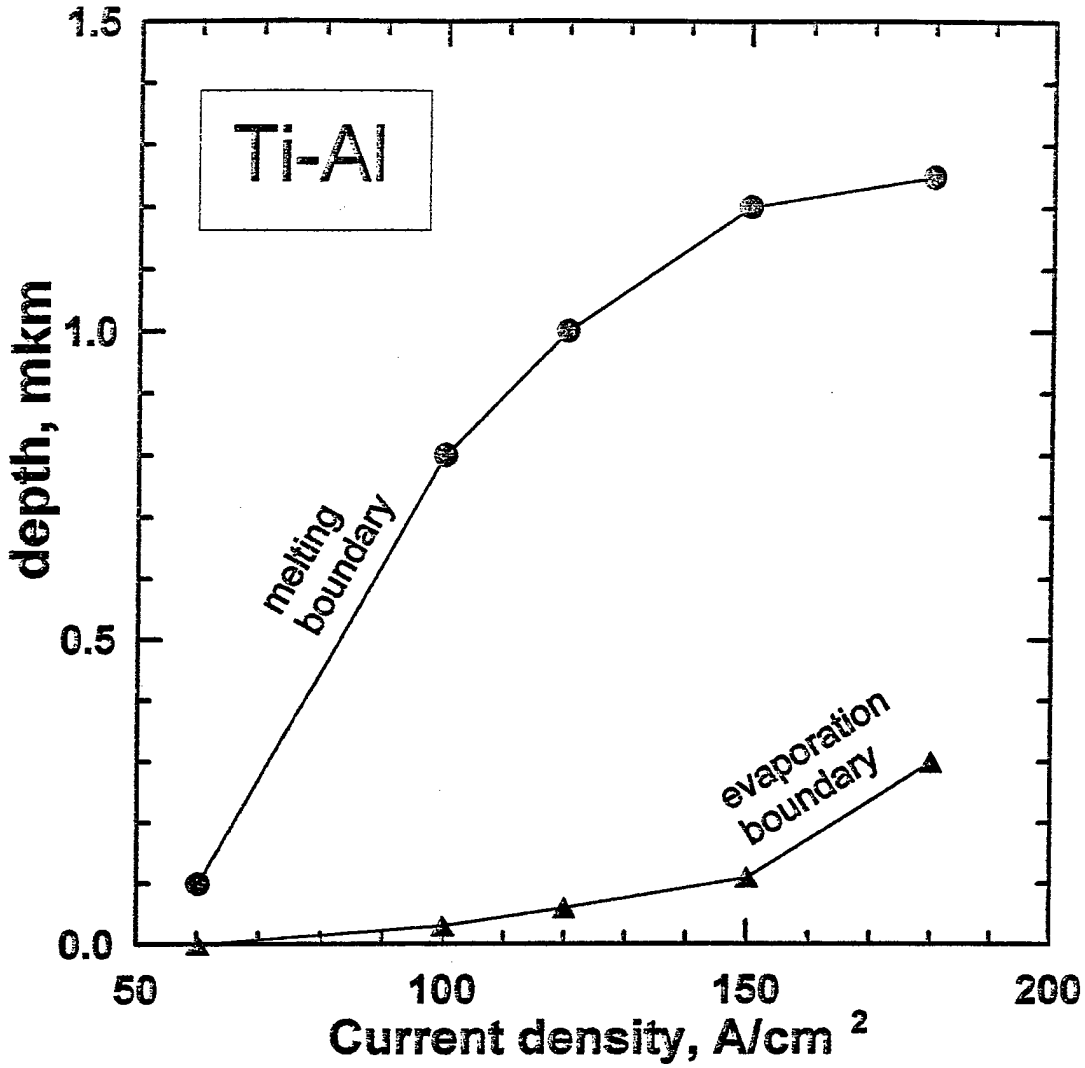
Ti-Al
depth, mkm
1.5
1.0
0.5
0.0
50
100
150
200
Current density, A/cm 2
melting boundary
evaporation boundary

FIG. 11

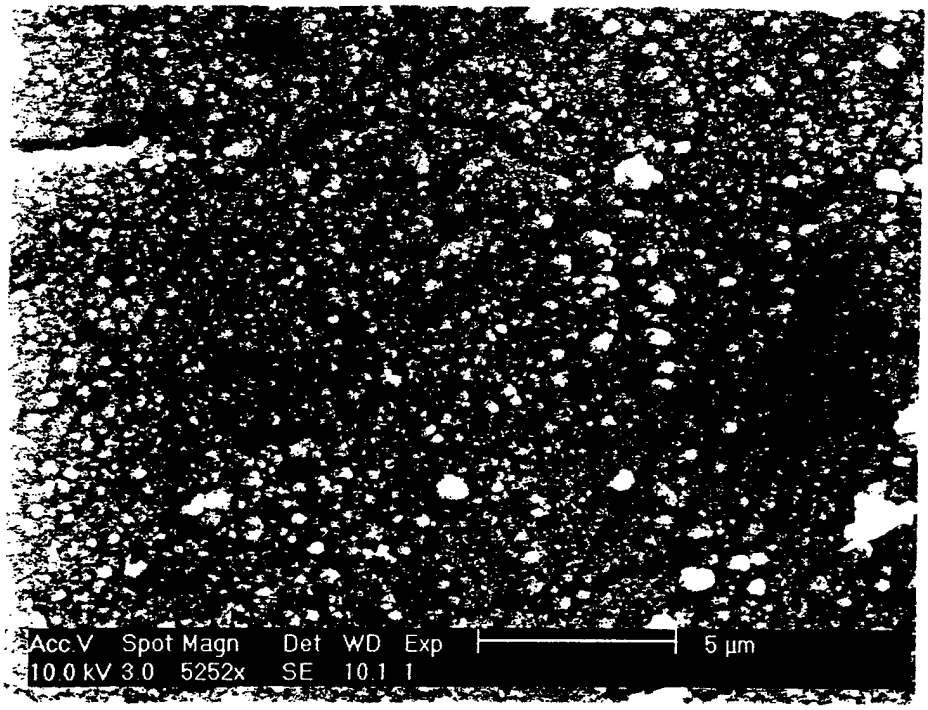
Acc.V Spot Magn Det WD Exp
10.0 kV 3.0 5252x SE 10.1 1
5 µm

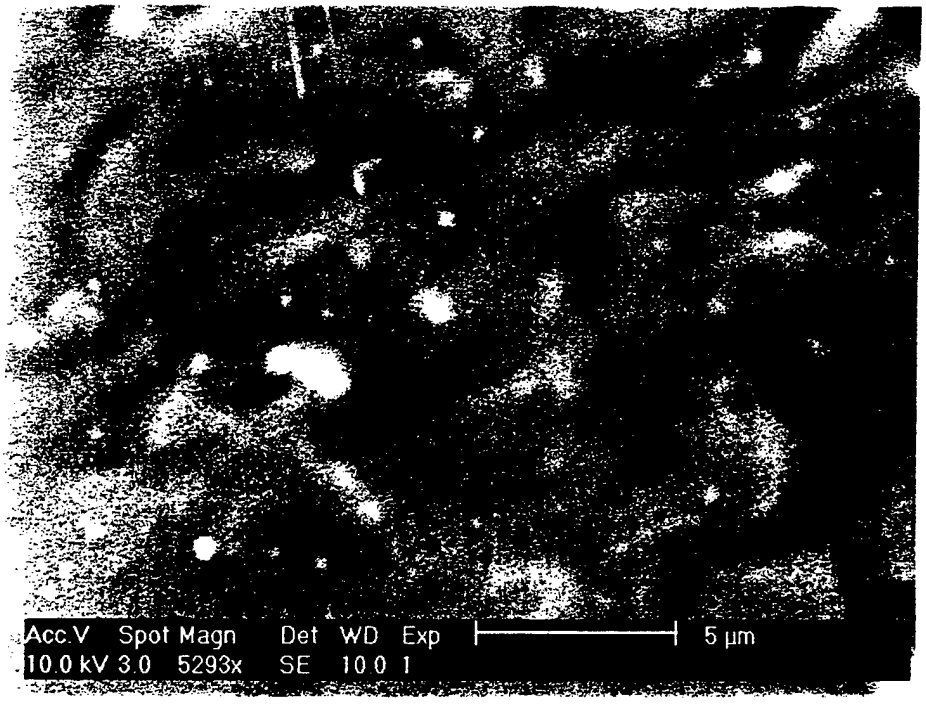
Acc.V Spot Magn Det WD Exp
10.0 kV 3.0 5293x SE 10.0 1
5 µm

FIG. 12

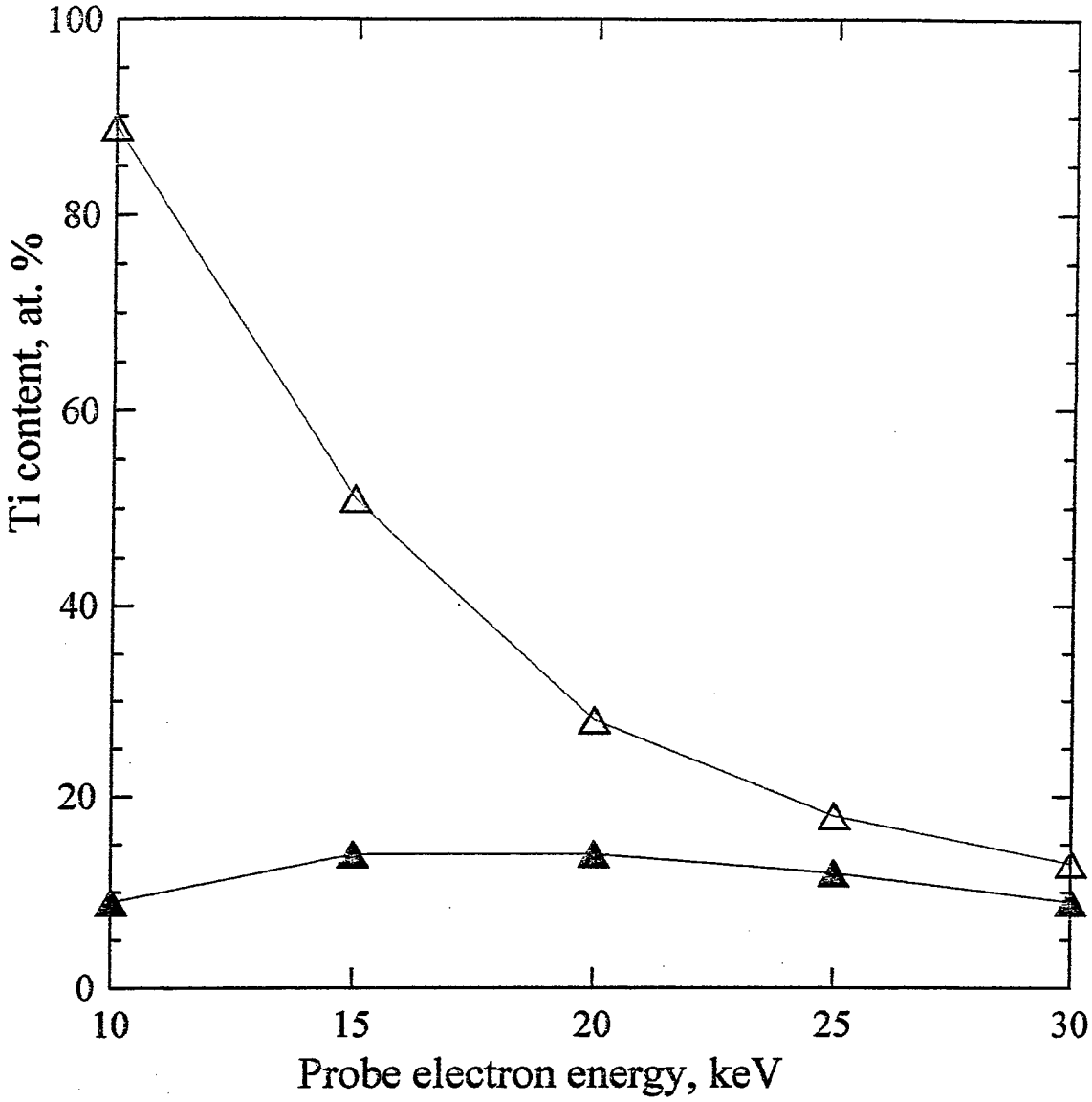
100
80
60
40
20
0
Ti content, at. %
10
15
20
25
30
Probe electron energy, keV

FIG. 13

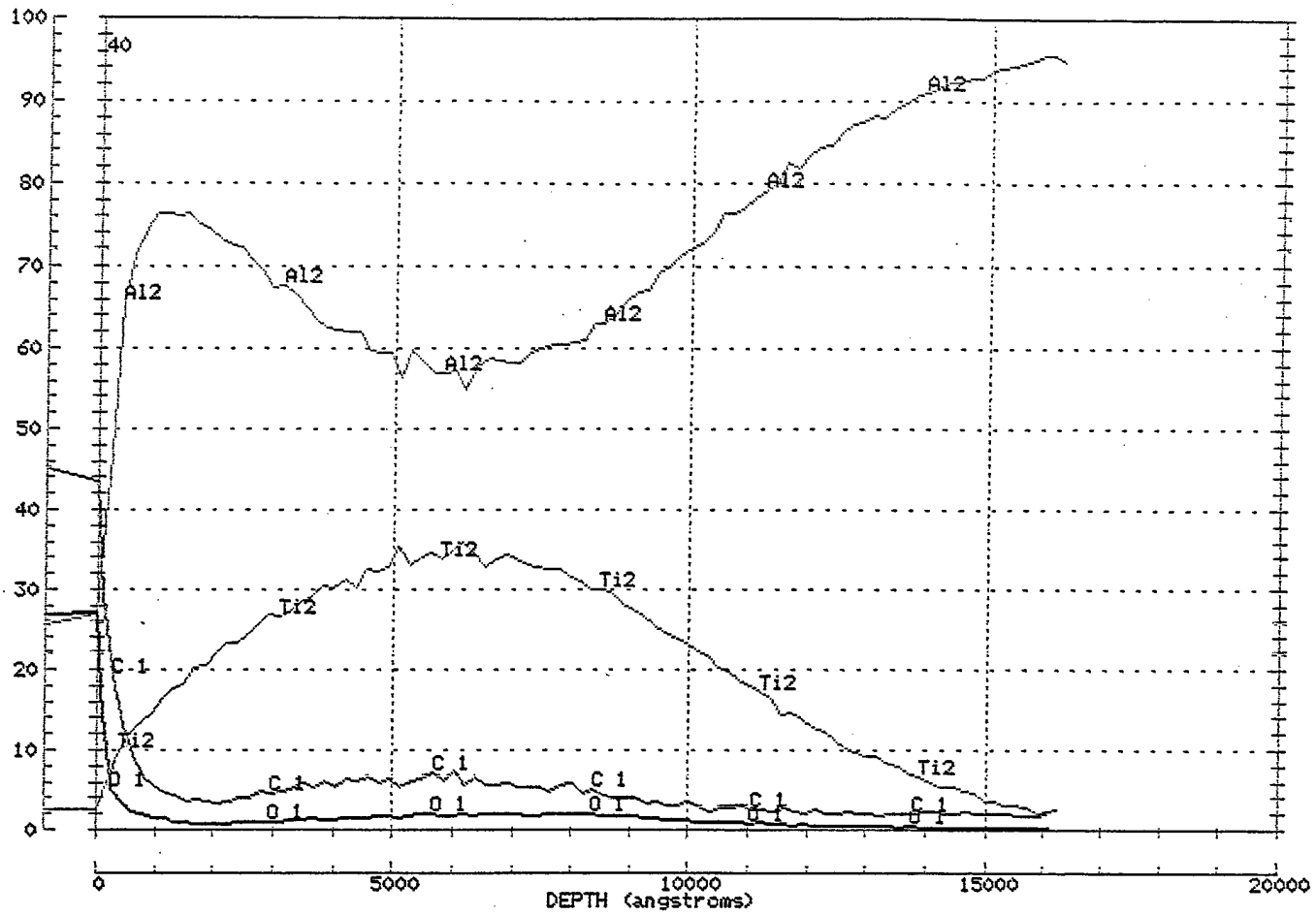
100
90
80
70
60
50
40
30
20
10
0
Al2
Ti2
C 1
O 1
0
5000
10000
15000
20000
DEPTH (angstroms)

FIG. 14

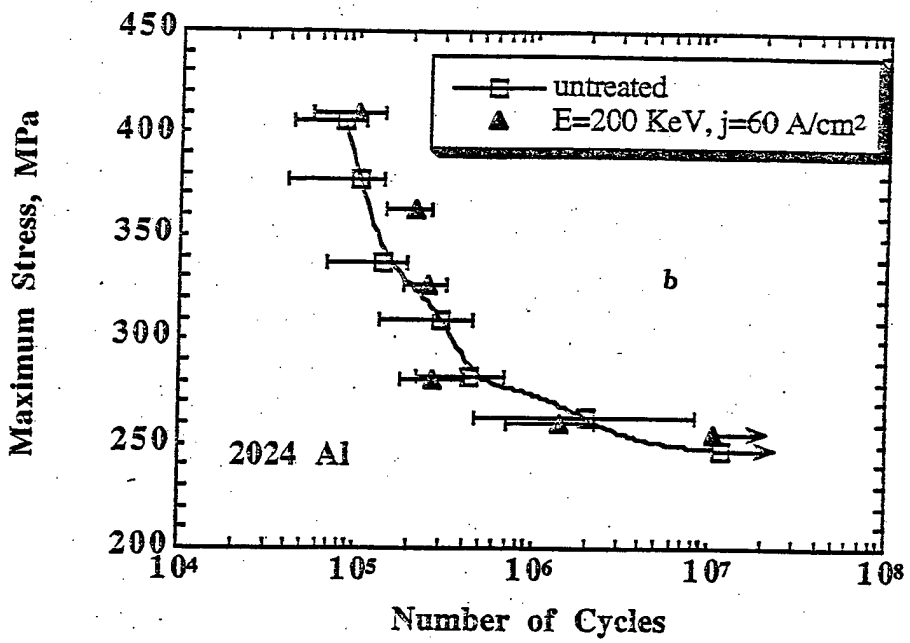

FIG. 15

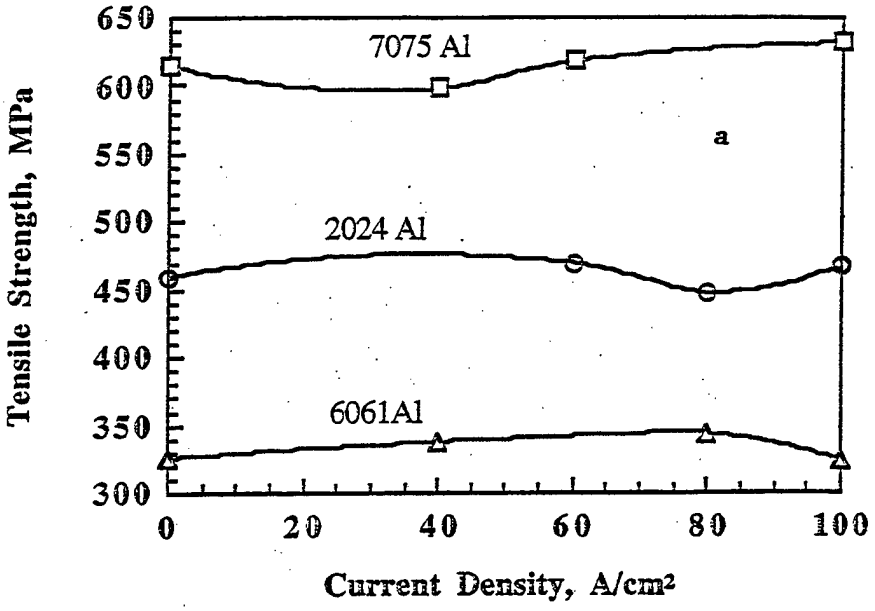

FIG. 15 Effect of the current density of ion beams on tensile strength of Al alloys

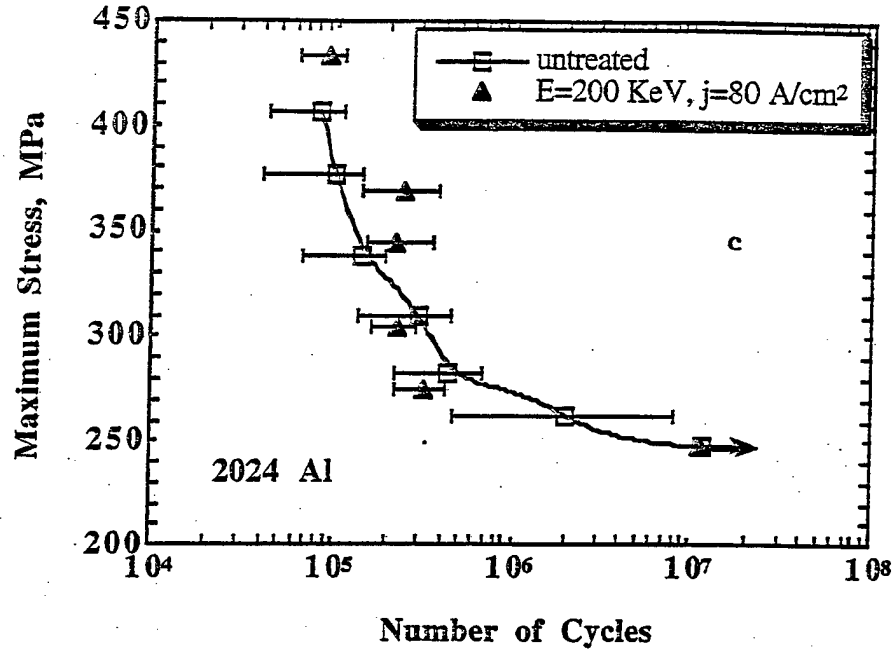

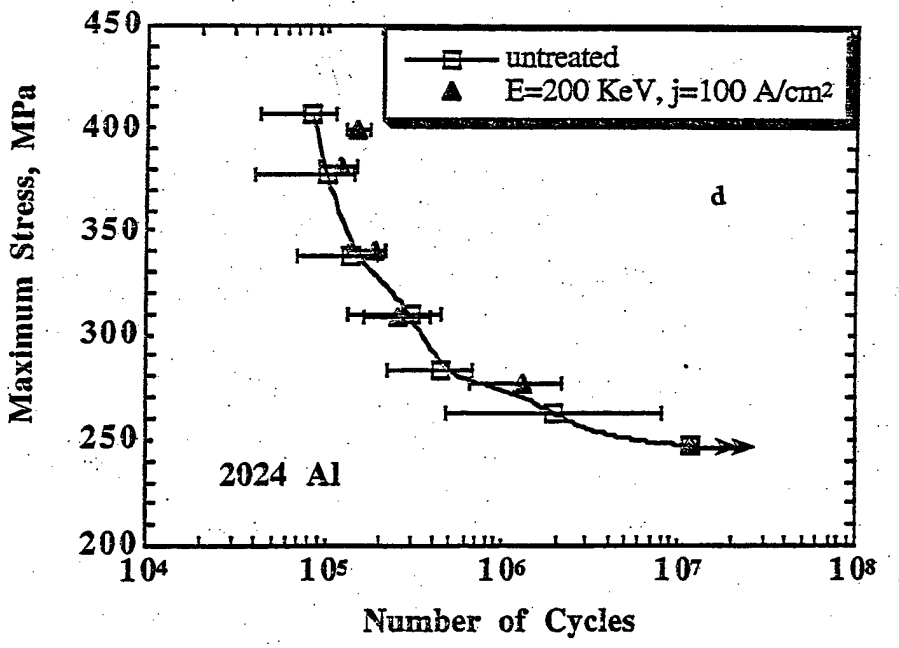

FIG. 15 S-N curves obtained from bending fatigue tests of 2024 Al alloy

Four-point bending fatigue
for Al7075-T6. R=0.1, f=30 Hz

Open circles- MPOS treated Al7075-T6
Closed circles- Nontreated Al7075-T6
in 0.5 M NaCl aqueous solution. The upper curve is air fatigue (statistically the same for treated and untreated samples)

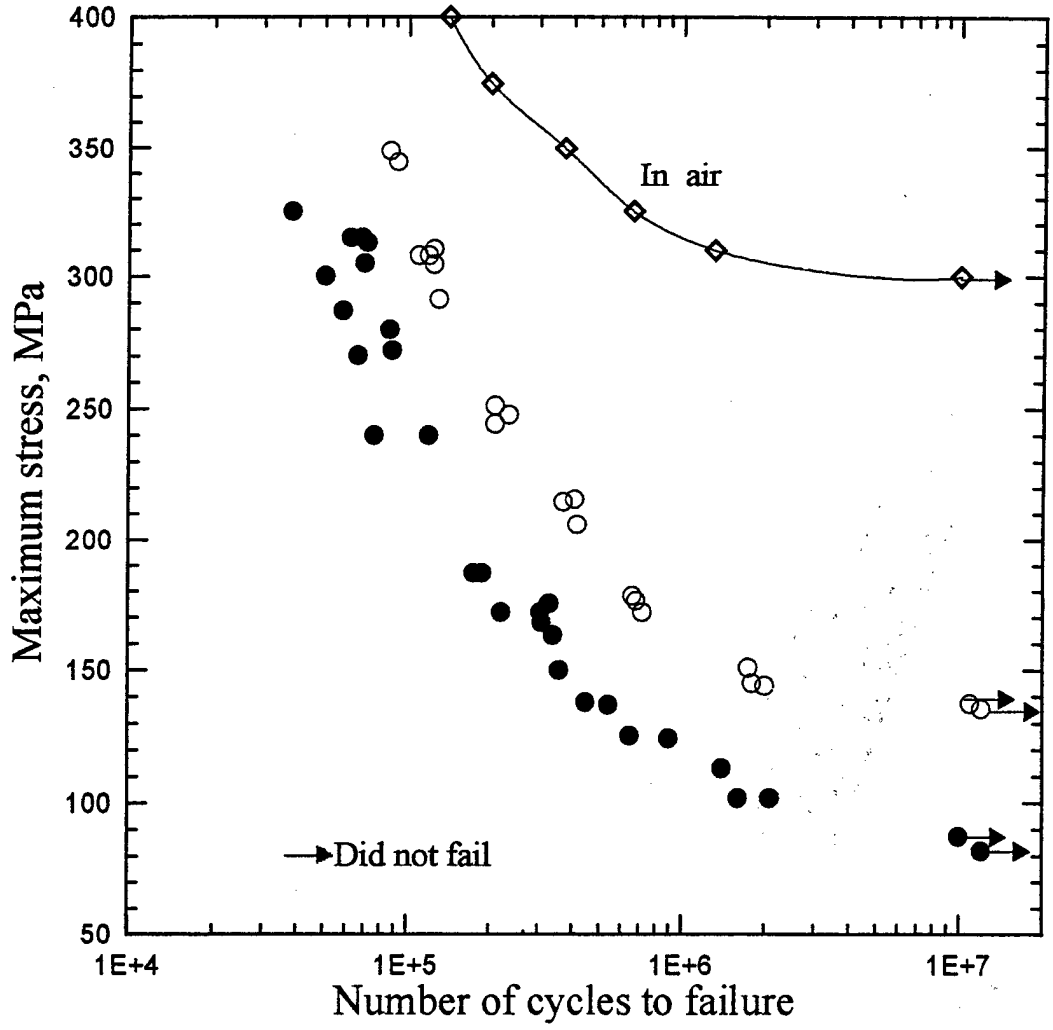

FIG. 16

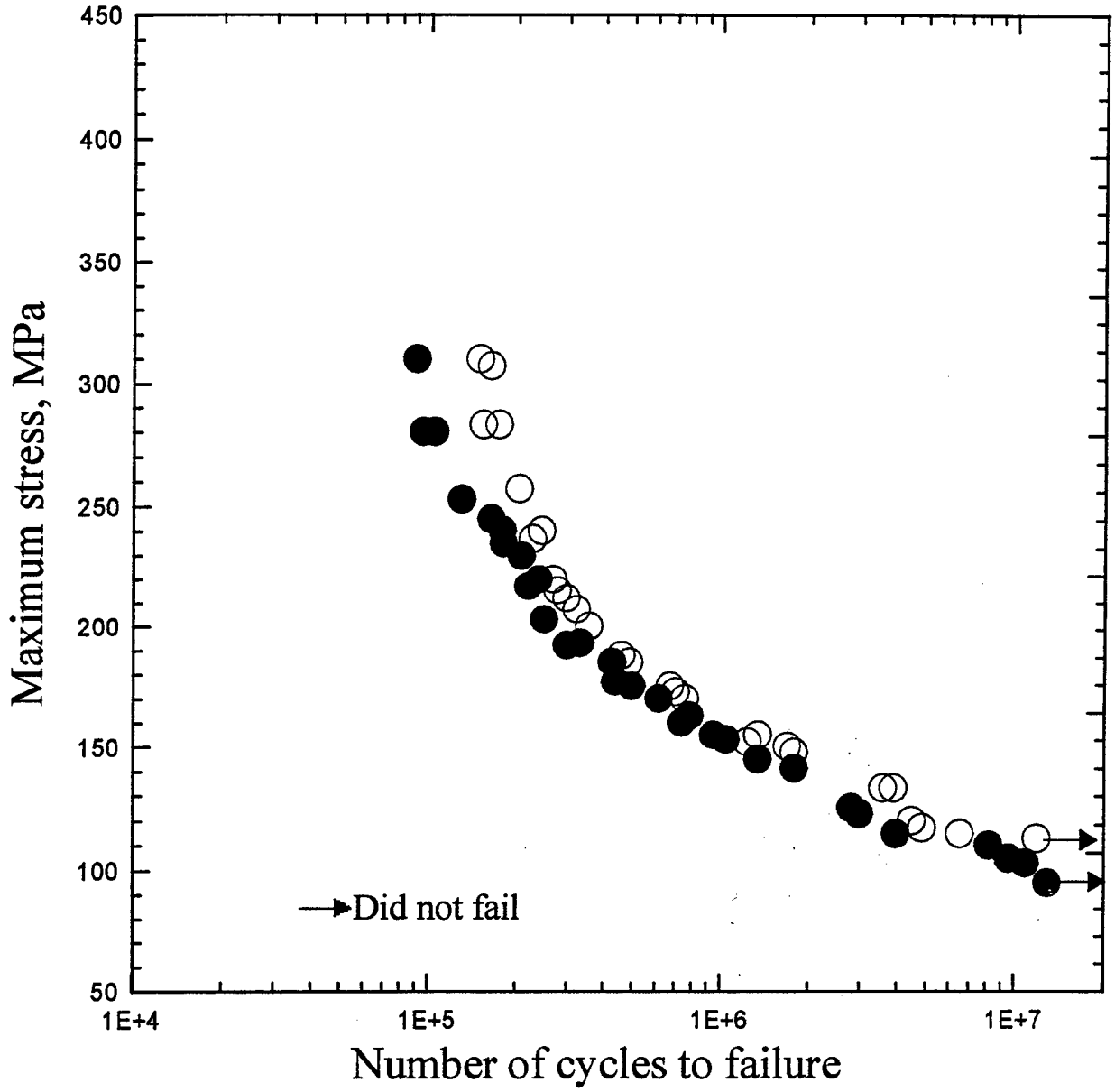
450
400
350
300
250
200
150
100
50
Maximum stress, MPa
1E+4
1E+5
1E+6
1E+7
Number of cycles to failure
Did not fail

FIG. 17

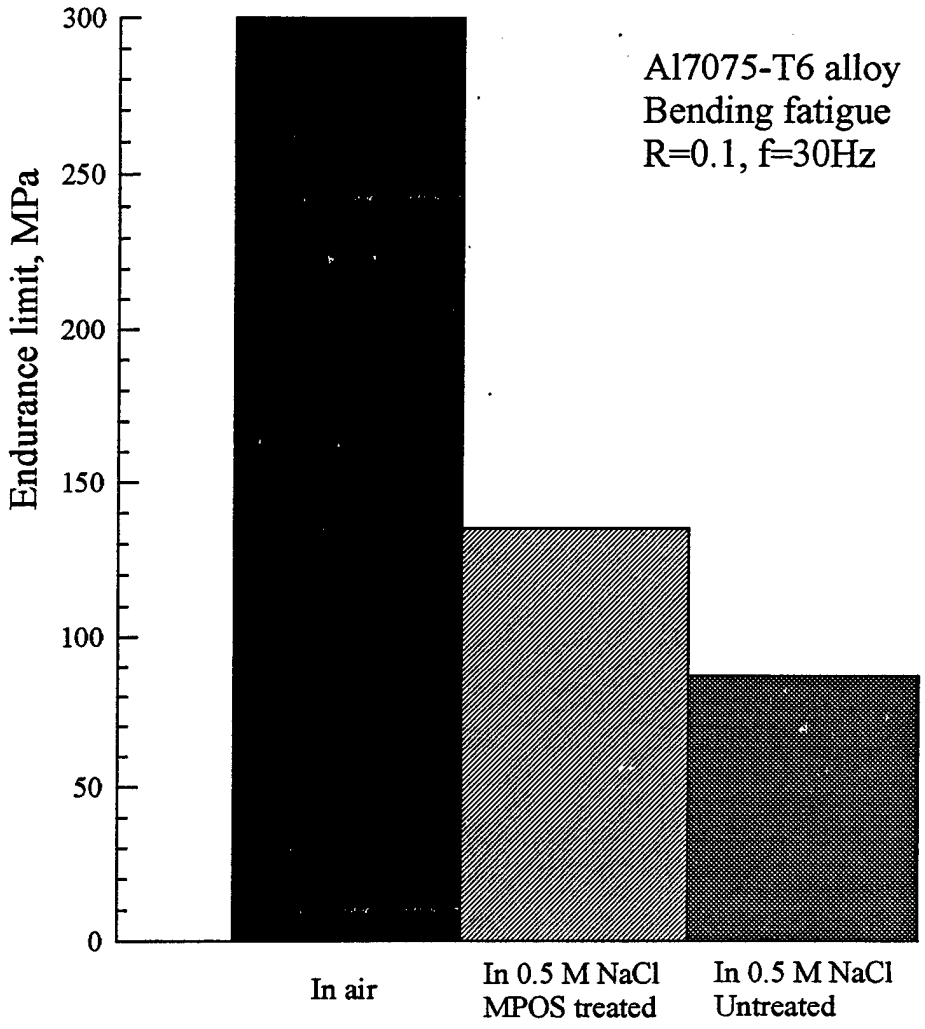
Al7075-T6 alloy
Bending fatigue
R=0.1, f=30Hz
Endurance limit, MPa
300
250
200
150
100
50
0
In air
In 0.5 M NaCl
MPOS treated
In 0.5 M NaCl
Untreated

FIG. 18